Human Molecular Genetics, 2020, Vol. 29, No. 17 2920–2935

doi: 10.1093/hmg/ddaa179
Advance Access Publication Date: 17 August 2020
General Article

GENERAL ARTICLE

Gene therapy for Alzheimer's disease targeting *CD33* reduces amyloid beta accumulation and neuroinflammation

Ana Griciuc[1], Anthony N. Federico[1], Jeyashree Natasan[2], Angela M. Forte[1], Danielle McGinty[1], Huong Nguyen[3], Adrienn Volak[2], Stanley LeRoy[2], Sheetal Gandhi[3], Eli. P. Lerner[3], Eloise Hudry[3,‡], Rudolph E. Tanzi[1,‡] and Casey A. Maguire[2,*,†,‡]

[1]Genetics and Aging Research Unit, McCance Center for Brain Health, MassGeneral Institute for Neurodegenerative Disease, Department of Neurology, Massachusetts General Hospital, Harvard Medical School, Charlestown, MA 02129, USA, [2]Molecular Neurogenetics Unit, Department of Neurology, Massachusetts General Hospital, Harvard Medical School, Charlestown, MA, 02114, USA and [3]Alzheimer's Disease Research Laboratory, MassGeneral Institute for Neurodegenerative Disease, Department of Neurology, Massachusetts General Hospital, Harvard Medical School, Charlestown, MA, 02129, USA

*To whom correspondence should be addressed. Tel: +617-726-5725; Email: cmaguire@mgh.harvard.edu

Abstract

Neuroinflammation is a key contributor to the pathology of Alzheimer's disease (AD). CD33 (Siglec-3) is a transmembrane sialic acid-binding receptor on the surface of microglial cells. CD33 is upregulated on microglial cells from post-mortem AD patient brains, and high levels of CD33 inhibit uptake and clearance of amyloid beta (Aβ) in microglial cell cultures. Furthermore, knockout of *CD33* reduces amyloid plaque burden in mouse models of AD. Here, we tested whether a gene therapy strategy to reduce *CD33* on microglia in AD could decrease Aβ plaque load. Intracerebroventricular injection of an adeno-associated virus (AAV) vector-based system encoding an artificial microRNA targeting *CD33* (miR^{CD33}) into *APP/PS1* mice reduced *CD33* mRNA and TBS-soluble Aβ40 and Aβ42 levels in brain extracts. Treatment of *APP/PS1* mice with miR^{CD33} vector at an early age (2 months) was more effective at reducing Aβ plaque burden than intervening at later times (8 months). Furthermore, early intervention downregulated several microglial receptor transcripts (e.g. *CD11c*, *CD47* and *CD36*) and pro-inflammatory activation genes (e.g. *Tlr4* and *Il1b*). Marked reductions in the chemokine Ccl2 and the pro-inflammatory cytokine Tnfα were observed at the protein level in the brain of *APP/PS1* mice treated with miR^{CD33} vector. Overall, our data indicate that CD33 is a viable target for AAV-based knockdown strategies to reduce AD pathology.

One Sentence Summary: A gene therapy approach for Alzheimer's disease using adeno-associated virus vector-based knockdown of *CD33* reduced amyloid beta accumulation and neuroinflammation.

[†]Casey A. Maguire, http://orcid.org/0000-0001-8681-5179
[‡]These authors contributed equally: Eloise Hudry, Rudolph E. Tanzi and Casey A. Maguire.
Received: May 4, 2020. **Revised:** July 3, 2020. **Accepted:** July 29, 2020

Introduction

The vast majority of elderly patients with dementia suffers from the late-onset form of Alzheimer's disease (AD), which is genetically complex with a heritability estimated above 80% (1,2). Over the past decade, genome-wide association studies performed on large cohorts of individuals and families have allowed the identification of numerous genetic variants associated with an increased risk to develop the disease or conferring resilience towards AD-related neurodegeneration. While most of the single nucleotide polymorphisms (SNPs) have a modest impact on the pathology, there is no doubt that these findings have led to a better understanding of the molecular mechanisms in play. In particular, while few of the genes potentially modulate the generation and aggregation of amyloid beta (Aβ) or formation of neurofibrillary tangles (NFT) that characterize the disease (3,4), a growing number of AD-associated gene variants are related to the innate immune system and microglial activities, including clearance of the neurotoxic Aβ (e.g. *CD33* (4,5), *TREM2*, *CR1* (6)). This observation suggests that not only the appearance and the accumulation of the typical AD lesions are of relevance but also the mechanisms through which the brain is able to cope with these injuries. As a consequence, these genetic findings give us a complex picture of the pathology that relies upon neuronal-dependent events at the same time as non-neuronal mechanisms involving microglial cells and their capacity at clearing Aβ species, managing NFT-dependent toxicity and controlling secondary neuroinflammatory processes.

Two SNPs in *CD33*, rs3826656 (5) and rs3865444 (7,8), have been associated with late-onset AD. CD33 is a type 1 transmembrane protein (Siglec-3) and is a member of the sialic acid-binding immunoglobulin-like lectins (Siglecs). CD33 has a sialic acid-binding V-type immunoglobulin-like domain (V-Ig), which recognizes sialic acids of glycoproteins and glycolipids, and immunoreceptor tyrosine-based inhibition motifs (ITIM) important for restricting immune responses (9). CD33 is expressed on the surface of immune cells (myeloid progenitor cells, monocytes, macrophages and others) where it regulates inflammatory responses of the innate immune system.

We identified CD33 as an important regulator of microglial function in AD (10). We showed, for the first time, that CD33 is prominently expressed in microglial cells in the brain. The numbers of CD33-positive microglia were markedly increased in AD relative to control brains and closely correlated with amyloid plaque burden in AD (10). The minor (T) allele of the *CD33* SNP, rs3865444, which confers protection against AD, was associated with reductions in both CD33 microglial expression and levels of insoluble Aβ42 in AD brain. We also found that primary microglial cells from *CD33* knockout mice displayed an increased uptake of Aβ42 in comparison to wild-type microglia. CD33 overexpression in BV2 microglial cell line strongly inhibited Aβ42 uptake, a process that requires the sialic acid-binding V-Ig domain of CD33. Finally, amyloid plaque burden was markedly reduced in *APP/PS1* transgenic mice in which *CD33* has been knocked out (10). Thus, CD33 activity in microglial cells promotes Aβ pathology and CD33 has emerged as a novel target for drug development in AD.

CD33 expression levels in the brain correlated with AD status and cognitive decline (11). An independent study also showed that increased expression of *CD33* mRNA was associated with increasing AD pathology in temporal cortex brain samples (12). The risk (C) allele of rs3865444 has been associated with increased expression of full-length CD33 and decreased Aβ42 uptake in circulating monocytes, as well as accumulation of fibrillar amyloid on *in vivo* imaging in human brain (13). Finally, the protective (T) allele of rs3865444 was associated with (i) decreased expression of full-length CD33 containing exon2/V-Ig domain in human brain and with (ii) increased levels of *CD33* splice variants that lack exon2/V-Ig domain or retain *CD33* intron 1 (14,15). Collectively, these findings suggest that CD33 might play a critical role in the etiology and pathogenesis of AD.

Recently, we showed that knockout of *CD33* attenuated Aβ pathology and neurodegeneration and improved cognition in 5x*FAD* transgenic mice, all of which were abrogated by additional knockout of the microglial receptor *TREM2* (16). RNA-seq profiling of microglia revealed that genes related to phagocytosis and signaling (IL-6, IL-8 and acute phase response) were upregulated in 5×*FAD*;*CD33*$^{-/-}$ mice. Remarkably, differential gene expression in 5×*FAD*;*CD33*$^{-/-}$ microglia depended on the presence of *TREM2*, suggesting TREM2 acts downstream of CD33. Crosstalk between CD33 and TREM2 in 5×*FAD* microglia included regulation of the IL-1β/IL-1RN axis and a gene set related to the receptor activity chemokine cluster (16). Thus, these findings pave the way for novel therapeutic approaches for the prevention and treatment of AD based on inhibition of CD33 and modulation of microglial activation state.

Gene therapy to treat central nervous system (CNS) and sensory rare genetic diseases using adeno-associated virus (AAV) vectors has led to impressive therapeutic results in clinical trials and in 2017 was Food and Drug Administration (FDA) approved for the treatment of a form of inherited blindness (17). Treating a broad AD population with gene therapy has been difficult owing to the multifactorial nature of the disease, with limited genetic targets available. Here we tested whether targeting murine *CD33* using a vector-delivered artificial microRNA (amiR) specific for CD33 (miR^{CD33}) could reduce amyloid burden in *APP/PS1* mice. Intracerebroventricular (ICV) injection of vector encoding miR^{CD33} or an identical vector encoding a control amiR was compared at reducing *CD33* mRNA, levels of soluble and insoluble Aβ species and amyloid plaque burden after early (2-month-old) or late (8-month-old) intervention in *APP/PS1* mice.

Results

Treatment of 8-month-old *APP/PS1* mice with vector-encoded artificial miR targeting *CD33* reduces TBS-soluble Aβ, but not amyloid plaque load

We designed an amiR targeting *CD33* (miR^{CD33}) or control miR using the miR-155 backbone construct as previously described (18). These miRs were separately cloned into an AAV expression plasmid containing a chicken beta actin (CBA) promoter after green fluorescent protein (GFP) cDNA allowing co expression of both the miR as well as GFP (Fig. 1A).

We then decided to test the efficiency of miR^{CD33}-mediated knockdown in cell culture assays. For this purpose, we generated HEK293T cells transduced by a lentivirus encoding mouse CD33 and mCherry fluorescent protein. To mimic a cell line with levels of mouse CD33 similar to those of microglia, we isolated a single cell clone line expressing low levels of mCherry, and thereby CD33, by using FACS-sorting and quantitative polymerase chain reaction (qPCR) screening for *CD33* transcript. Subsequently, we transfected the single cell clone line expressing low levels of mouse CD33 (HEK293T-mCD33) with miR control or miR^{CD33} AAV expression plasmids. Seventy-two hours post-transfection, we isolated RNA from cell lysates and performed qPCR analysis on the mouse *CD33* transcript. We found that miR^{CD33} led to a 32.11% knockdown ($P < 0.0001$) of *CD33* transcript in comparison to miR control in HEK293T-mCD33 cells (Fig. 1B).

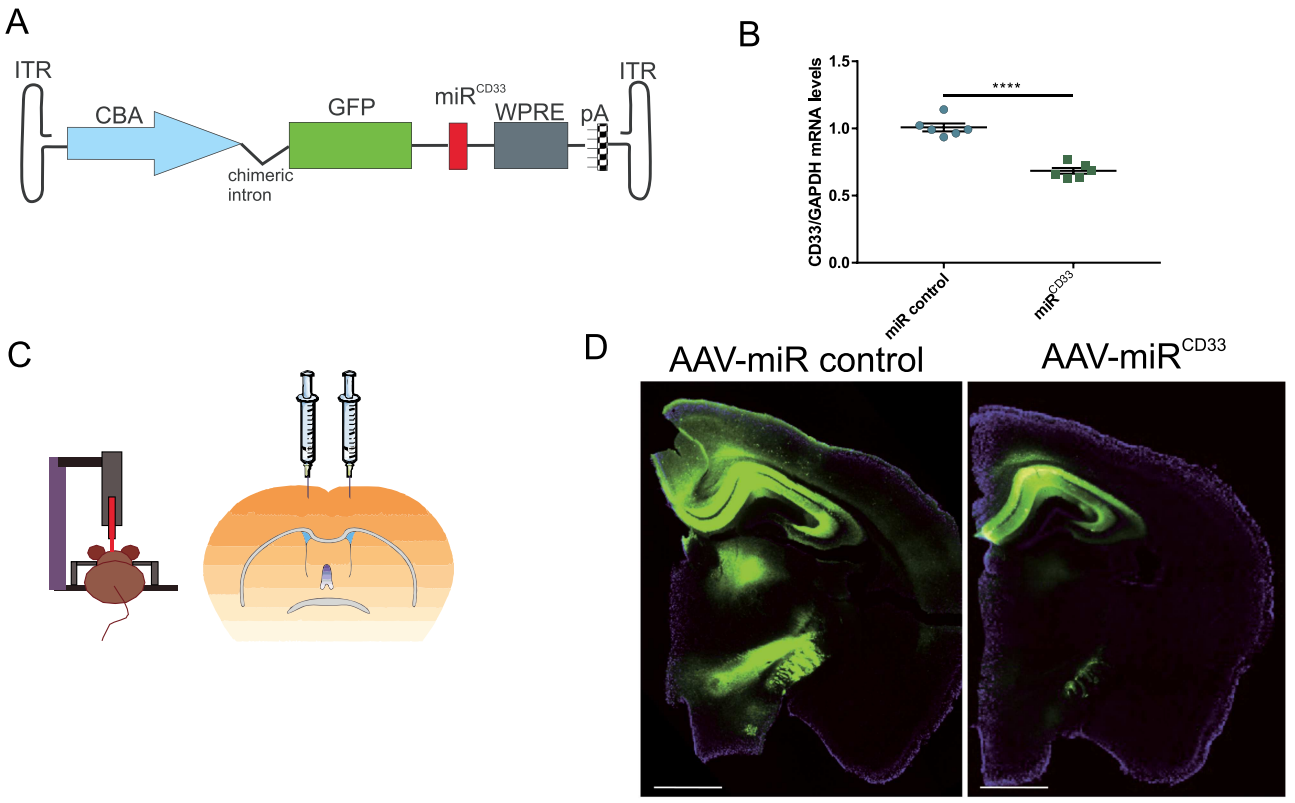

Figure 1. Schematic representation of miR control and miR^{CD33} vector injections in *APP/PS1* mice. (**A**) AAV vector encoding miR targeting *CD33* (miR^{CD33}). The construct also encodes GFP allowing visualization of transduction efficiency in the brain. CBA, CMV IE enhancer/chicken beta actin hybrid promoter; WPRE, woodchuck hepatitis virus posttranscriptional regulatory element; pA, polyA signal; ITR, inverted terminal repeat. (**B**) RNA was extracted from a single cell clone HEK293T line stably expressing mouse CD33 that was transfected with miR control or miR^{CD33} AAV expression plasmids. RNA was used to measure *CD33* expression levels normalized to *GAPDH* transcripts. *CD33* mRNA levels were reduced by 32.11% (****$P < 0.0001$, unpaired *t* test with Welch's correction) in cells transfected with miR^{CD33} compared to miR control. Data are represented as mean ± SEM. (**C**) Schematic representation of treatment: vectors were injected into both lateral ventricles of *APP/PS1* mice. (**D**) Representative images of the GFP signal detected in brain sections from mice injected with control vector or vector encoding miR^{CD33}. Scale bar represents 1000 µm. See also Supplementary Material, Figure S1.

Next, we produced exosome-associated AAV serotype 9 vectors (exo-AAV9) encoding miR^{CD33} or miR control (exo-AAV9-miR^{CD33}, or exo-AAV9-miR control). We generated exo-AAV9 vectors as we (19) and others (20) have found that AAV can associate with exosomes and provide robust transgene expression *in vivo* (21) including the CNS (22,23). Furthermore, they are technically less laborious to produce as compared to standard AAV vectors, making them a useful tool in early preclinical research. Eight-month-old *APP/PS* mice were injected into both lateral ventricles with a total of 8×10^{10} GC of either exo-AAV9-miR^{CD33} ($n = 9$) or exo-AAV9-miR control ($n = 10$ group) (see schematic Fig. 1C).

Next, mice were aged for an additional 3 months and sacrificed at 11 months of age. From one hemisphere we extracted two 1-mm slices of brain spanning the ventricles, one for RNA isolation and one for quantitation of Aβ levels. From the other hemisphere we made cryosections for stereological quantitation of plaques (also from slices surrounding the ventricles). We first confirmed successful injections by immunostaining cryosections for GFP expression and found that both exo-AAV9-miR^{CD33} and exo-AAV9-miR control injected mice had robust GFP expression (mainly in neurons and astrocytes) around the ventricles (Fig. 1D). In the representative images shown, exo-AAV9-miR control resulted in higher GFP expression compared to exo-AAV9-miR^{CD33}. This is likely due to the variability of transduction efficiency, which essentially reflects the inter-individual variability of the surgical procedure (ICV infusions are technically challenging in small species such as mice). In the future, we could attempt to intravenously inject the newly developed AAV-F vector (a potent AAV9 variant recently identified by directed capsid evolution) (24) encoding miR to achieve a more evenly spread and robust transduction throughout the brain.

We next asked which cell types were transduced by exo-AAV9-miR control and exo-AAV9-miR^{CD33} in the *APP/PS1* mouse brain. Immunolabeling of mouse brain sections with a GFP-specific antibody (for miR control or miR^{CD33}) and markers for neurons (NeuN), astrocytes (glutamine synthetase, GS) and microglia (Iba1) revealed that miR control and miR^{CD33} transduced neurons and astrocytes, but not microglial cells (Supplementary Material, Fig. S1). Thus, these results suggest that any effect of miR^{CD33} would likely emerge from cross-correction from either neurons and/or astrocyes to microglia.

To assess whether miR^{CD33} could functionally reduce *CD33* mRNA levels, we performed an RT-qPCR on RNA isolated from tissue spanning the ventricles. We observed a 36.5% decrease (albeit non-significant, $P = 0.167$) in *CD33* mRNA levels in miR^{CD33}-treated mice compared to controls (Fig. 2A). Next, we used ELISA and an Aβ peptide panel based on the Meso Scale Discovery multi-spot assay system to detect the levels of Aβ peptides in TBS-soluble and formic acid (FA)-soluble fractions of brain tissue around the injection site, respectively. We observed a 30.1% (albeit non-significant, $P = 0.1117$) and 35.1% ($P = 0.0279$) decrease in TBS-soluble Aβ40

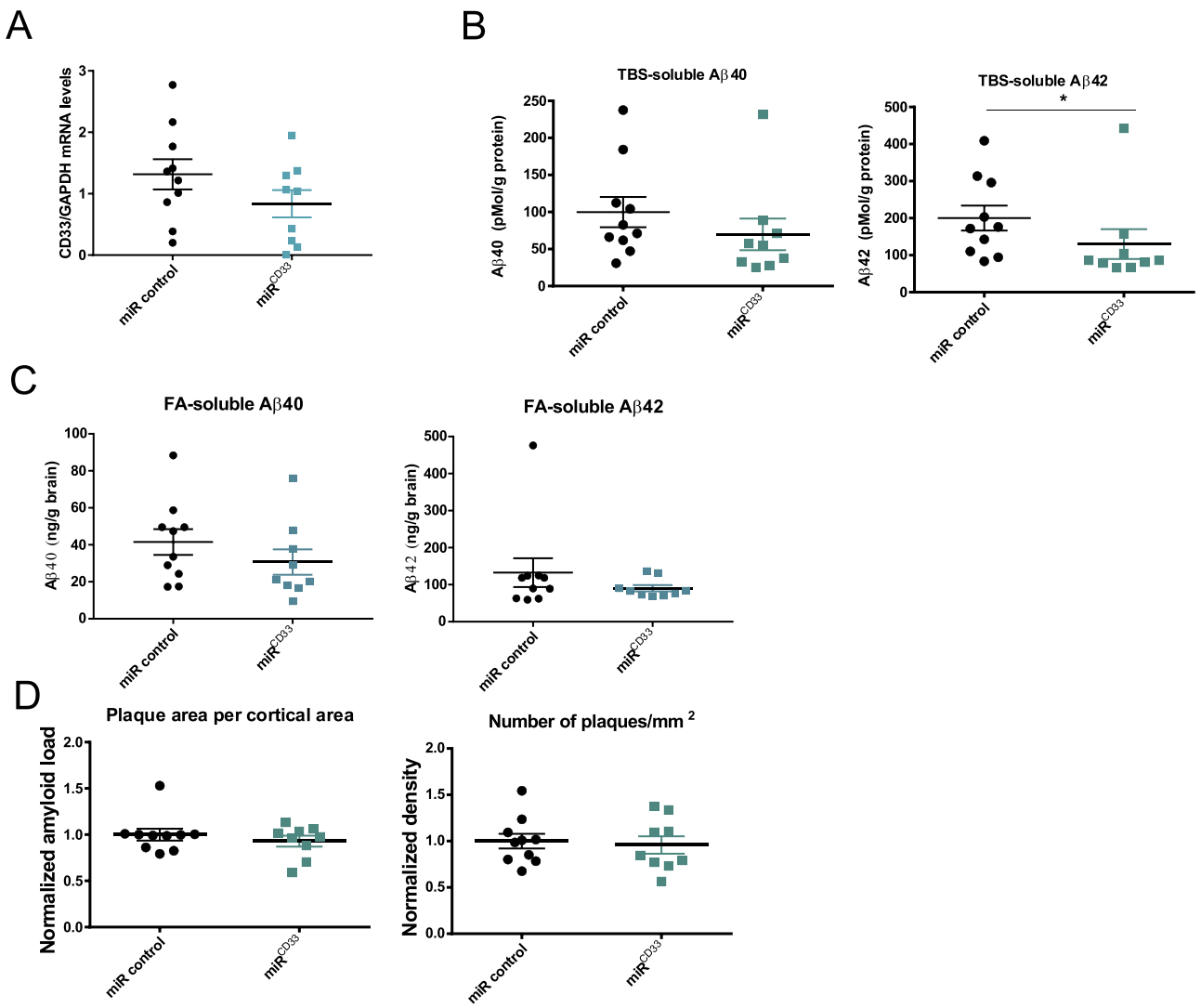

Figure 2. *CD33* mRNA expression and TBS-soluble Aβ levels, but not amyloid plaque burden, are decreased in the brain of *APP/PS1* mice by AAV-miR^{CD33} (late intervention). **(A–D)** Eight-month-old mice were injected into the lateral ventricles with AAV-miR control or AAV-miR^{CD33} and sacrificed at 11 months of age. (A) RNA was extracted from brain around the injection site and was used to measure *CD33* expression levels normalized to *GAPDH* transcripts. *CD33* mRNA levels were decreased by 36.5% (albeit non-significant, $P = 0.167$) in miR^{CD33}-treated *APP/PS1* mice compared to control mice. (B) and (C). ELISA (B) and Meso Scale Discovery multi-spot assay (C) of Aβ40 and Aβ42 peptides in TBS-soluble (B) or formic acid (FA)-soluble (C) fractions isolated from mouse brain tissue spanning the injection site. (B) Treatment with miR^{CD33} compared to control vector leads to decreased levels of TBS-soluble Aβ40 (30.1% decrease, $P = 0.1117$) and Aβ42 (35.1% decrease, $*P = 0.0279$) in *APP/PS1* mice. (C) Modest but non-significant reductions in FA-soluble levels of Aβ40 and Aβ42 were observed in *APP/PS1* mice treated with miR^{CD33} versus control vector. (D) Aβ plaque load quantitated stereologically in brain sections that were labeled with an antibody directed against Aβ. Plaque area and plaque density were assessed in both mouse groups, and data were normalized to the miR control group. Symbols in graphs represent individual animals ($n = 10$ for miR control, $n = 9$ for miR^{CD33}). Data are represented as mean ± SEM.

and Aβ42, respectively, in the miR^{CD33}-treated mice compared to controls (Fig. 2B). We observed modest but non-significant reductions in FA-soluble Aβ40 and Aβ42 by 26% ($P = 0.2428$) and 31.8% ($P = 0.7802$), respectively (Fig. 2C). Finally, to assess the effect of miR^{CD33} on Aβ deposition in the *APP/PS1* brain, we stained coronal sections from both mouse groups with an antibody directed against Aβ. We stereologically quantitated plaque load using two different parameters, plaque area and plaque density. In both parameters, plaque load was virtually identical between miR^{CD33} and miR control treated animals (Fig. 2D). Thus, late injection of miR^{CD33} vector compared to miR control led to a marked reduction in TBS-soluble Aβ42, but not amyloid plaque burden in the brains of *APP/PS1* mice.

Treatment of 2-month-old *APP/PS1* mice with vector-encoded artificial miR targeting *CD33* reduces TBS-soluble Aβ and amyloid plaque load

We next set out to test whether an earlier intervention with miR^{CD33} would allow for a better modulation of plaque load. To this end, we injected 2-month-old *APP/PS1* mice ICV with exo-AAV9-miR^{CD33} ($n = 9$) or exo-AAV9-miR control ($n = 8$) at a dose of 7.5×10^{10} total GC and sacrificed mice at 10 months of age. As in our initial experiment for late intervention reported in Fig. 2A, we isolated tissue spanning the ventricles and found that *CD33* mRNA levels were decreased by 30.1% ($P = 0.0107$) in the miR^{CD33} relative to miR control group for the early intervention approach (see Fig. 3A). In TBS-soluble brain extracts, Aβ40 and

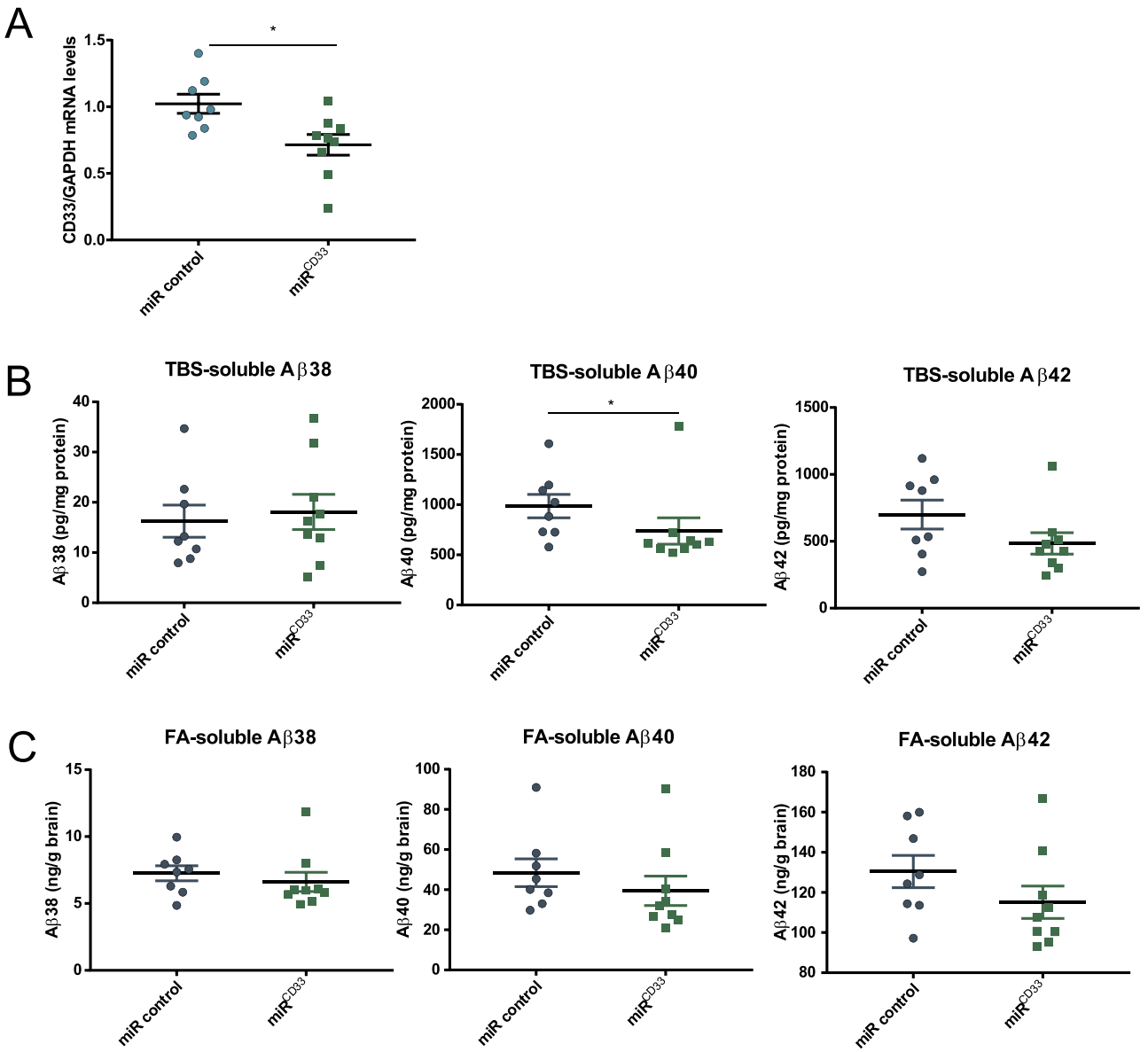

Figure 3. Early intervention therapy decreases *CD33* mRNA levels and TBS-soluble Aβ levels in *APP/PS1* mice. Two-month-old *APP/PS1* mice were injected into the lateral ventricles with vector encoding miR control or miR^{CD33} and sacrificed at 10 months of age for analysis. (**A**) Levels of *CD33* mRNA were significantly reduced with miR^{CD33} versus miR control (30.1% decrease, $*P = 0.0107$, unpaired *t* test with Welch's correction) in *APP/PS1* mice. (**B**) and (**C**) Meso Scale Discovery multi-spot assay of Aβ38, Aβ40 and Aβ42 peptides in TBS-soluble (B) or formic acid (FA)-soluble (C) fractions isolated from mouse brain tissue around the injection site. (B) TBS-soluble Aβ38 levels were comparable in both mouse groups. Early injection with miR^{CD33} versus miR control led to decreased levels of TBS-soluble Aβ40 (25.1% decrease, $*P = 0.0274$, Mann–Whitney test) and Aβ42 (30.8% decrease, $P = 0.1996$) in *APP/PS1* mice. (C) Levels of FA-soluble Aβ38 were similar in both mouse groups. Modest but non-significant reductions in FA-soluble Aβ40 and Aβ42 were noticed in miR^{CD33}-treated mice compared to control mice. Symbols in graphs represent individual animals ($n = 8$ for miR control, $n = 9$ for miR^{CD33}). Data are represented as mean ± SEM. See also Supplementary Material, Figure S2.

Aβ42 levels were decreased by 25.1% ($P = 0.0274$) and 30.8% (albeit non-significant, $P = 0.1996$), respectively, in miR^{CD33}-treated mice compared to control mice (Fig. 3B). In FA-soluble fractions, we observed modest but non-significant reductions in Aβ40 and Aβ42 levels by 18.6% ($P = 0.1672$) and 11.7% ($P = 0.1991$), respectively, in miR^{CD33}-treated mice versus miR control (Fig. 3C). Both TBS-soluble and FA-soluble Aβ38 levels were closely comparable between miR^{CD33} and control groups (Fig. 3B and 3C). Thus, treatment of *APP/PS1* mice with miR^{CD33} vector significantly decreased levels of TBS-soluble Aβ40 and non-significantly reduced TBS-soluble Aβ42 in *APP/PS1* mice.

We also generated detergent-soluble fractions that we used for subsequent western blotting assays. Using western blotting and an APP-specific antibody (10), we found comparable levels of full-length APP and APP C-terminal fragments (β-CTF and α-CTF) in both miR control and miR^{CD33}-treated *APP/PS1* mice (Supplementary Material, Fig. S2). Thus, these results show that miR^{CD33} treatment does not impact APP levels or APP processing in comparison to miR control in *APP/PS1* mice. Collectively, these data suggest that *APP/PS1* mice treated with miR^{CD33} versus miR control display reduced Aβ levels and plaque burden due to microglia-mediated clearance of Aβ.

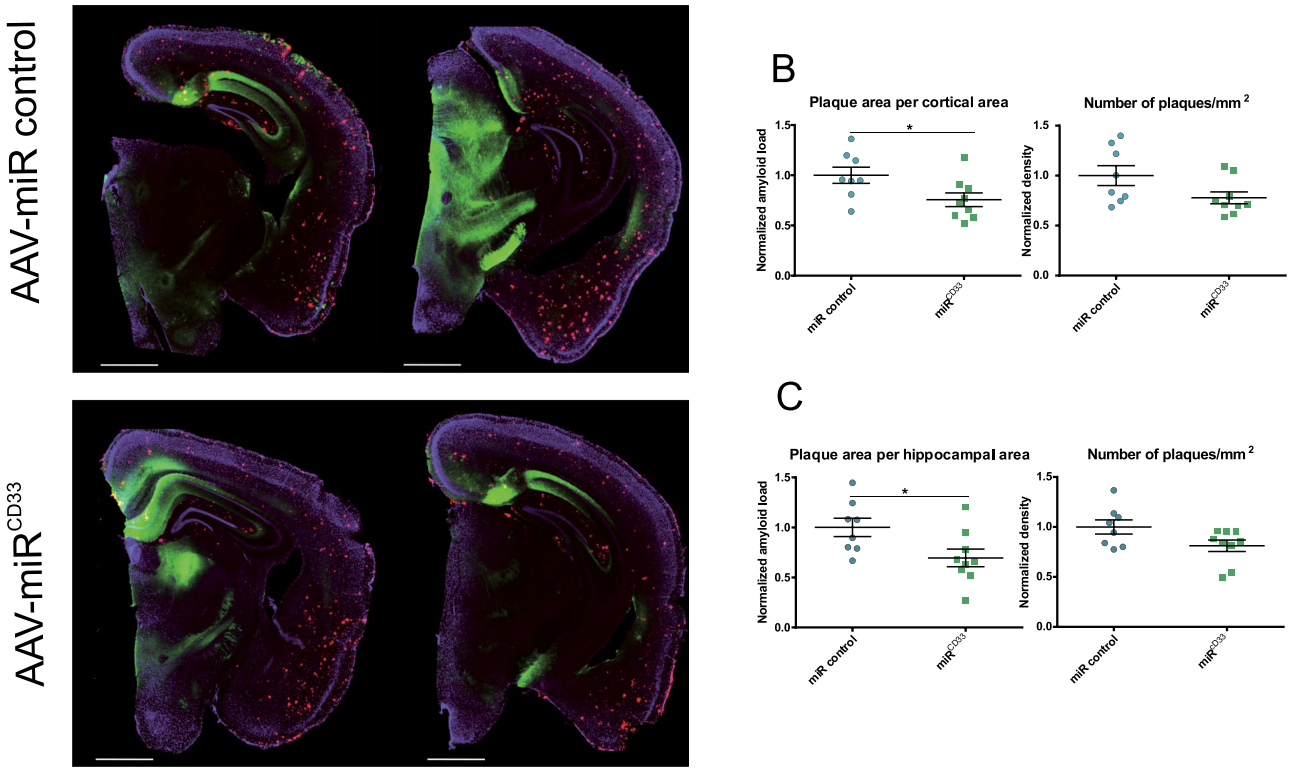

Figure 4. Early intervention therapy decreases amyloid plaque burden in *APP/PS1* mice. Two-month-old *APP/PS1* mice were injected into the lateral ventricles with vector encoding miR control or miR^{CD33} and sacrificed at 10 months of age. (**A**) Photomicrographs of selected coronal brain sections labeled with an antibody targeting Aβ (red, rabbit polyclonal antibody specific for the N-terminal fragment of Aβ) to reveal plaques and an anti-GFP antibody (green, chicken polyclonal antibody specific to GFP) to visualize the transduction efficiency and expression of miR control and miR^{CD33} vectors in the brain of *APP/PS1* mice. Brain sections were also counterstained with DAPI (blue). Scale bar represents 1000 µm. (**B** and **C**) Quantification of amyloid plaque area and plaque density in the cortex (B) and hippocampus (C) of *APP/PS1* mice treated with miR control or miR^{CD33} vector. Treatment with miR^{CD33} versus control vector decreased amyloid plaque burden as measured by area (24.4% decrease, $^*p = 0.035$, Unpaired *t* test with Welch's correction) and density (22.2% decrease, $p = 0.066$) in the cortex of *APP/PS1* mice. Treatment with miR^{CD33} versus miR control also reduced amyloid plaque burden in the hippocampus of *APP/PS1* mice. Symbols in graphs represent individual animals ($n = 8$ for miR control, $n = 9$ for miR^{CD33}). Data are represented as mean ± SEM. See also Supplementary Material, Figures S3 and S4.

Next, we stained coronal sections of mouse brains with an antibody targeting Aβ to assess plaque levels, and with a GFP-specific antibody to visualize the transduction efficiency and expression of miR control and miR^{CD33} vectors in the brain (Fig. 4A). The staining with the anti-GFP antibody confirmed that all the mice had been successfully injected and both miR control and miR^{CD33} vectors were expressed at similar levels in *APP/PS1* mice (Fig. 4A). Stereological quantitation of Aβ plaque load in the cortical area revealed a reduction in plaque area of 24.4% ($P = 0.035$) and a trend for reduction in plaque density of 22.2% ($P = 0.066$) in miR^{CD33}-treated mice relative to controls (Fig. 4B). Similar results were obtained in the hippocampal area, displaying a reduction in plaque area of 30.52% ($P = 0.0206$) and a trend for reduction in plaque density of 18.8% ($P = 0.056$) in miR^{CD33}-treated mice relative to controls (Fig. 4C). We also quantified the level of association of microglia with amyloid plaques. Amyloid plaques were labeled with methoxy-X04, and microglia were labeled with the microglial marker Iba1 (Supplementary Material, Fig. S3) or a marker of activated phagocytic microglia, CD68 (Supplementary Material, Fig. S4). Measurements of the ratio of microglia/plaque association were made in both the cortex and hippocampus for both miR control and miR^{CD33}-treated animals. No statistically significant difference in the ratio of Iba1-positive or CD68-positive microglia to plaques was observed in either region in miR^{CD33}-treated mice versus control mice (Supplementary Material, Figs S3 and S4). Collectively, our results show that early injection of miR^{CD33} vector leads to reduced Aβ plaque burden but does not impact microglial clustering around amyloid plaques in *APP/PS1* mice, versus control vector.

Transcript and protein analyses of miR^{CD33}-treated *APP/PS1* mice in comparison to control mice reveal changes in neuroinflammation

To analyze whether miR^{CD33} treatment altered transcripts associated with neuroinflammation compared to the control vector, we performed an reverse transcriptase-quantitative polymerase chain reaction (RT-qPCR) array of 14 transcripts normalized to *GAPDH*. The panel of 14 transcripts included microglial phagocytosis-related genes and pro- and anti-inflammatory activation genes. We also included *CD33* in the panel to validate our earlier data. We observed a 33.41% reduction in *CD33* mRNA levels ($P = 0.0078$) in mice treated with miR^{CD33} compared to miR control (Fig. 5). Surprisingly,

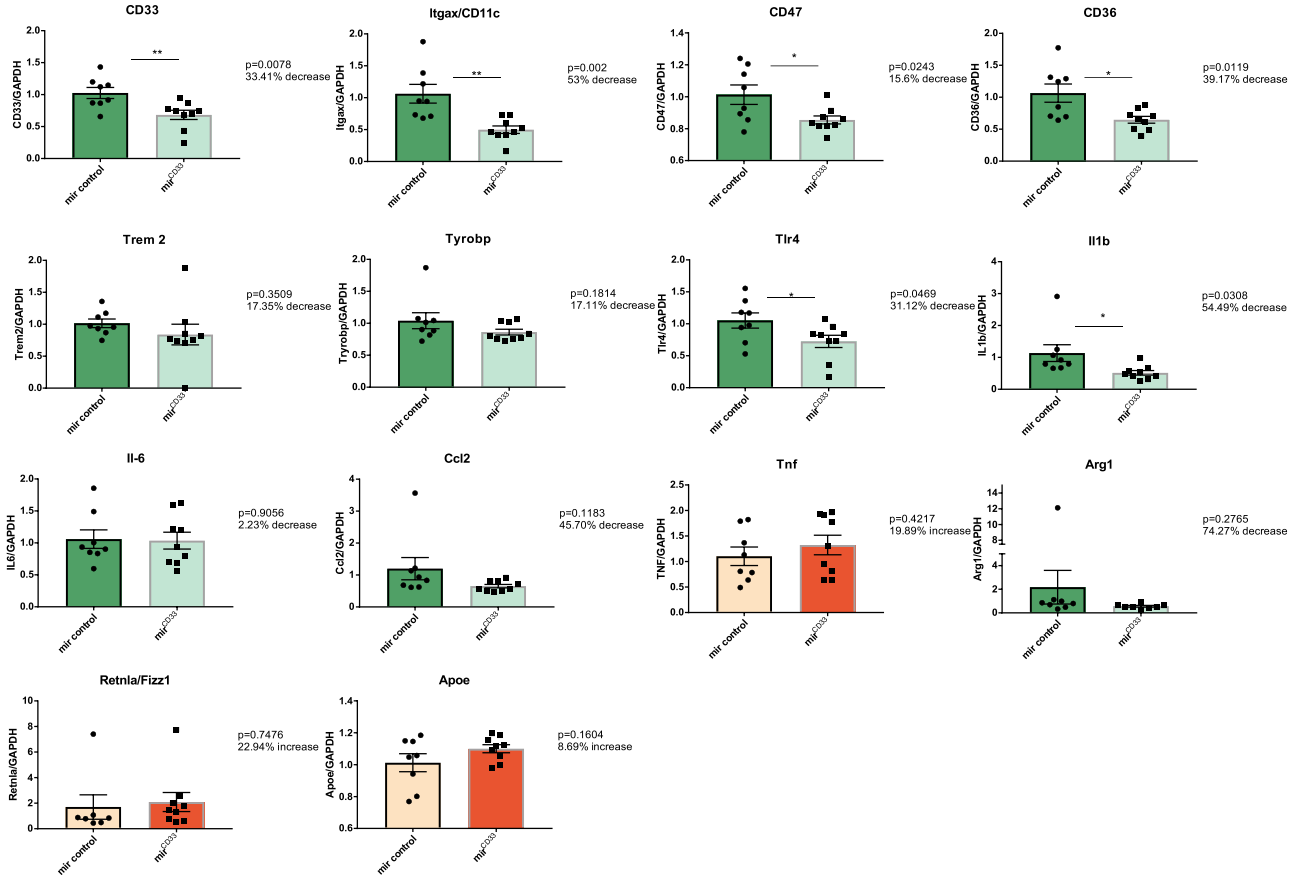

Figure 5. PCR array analysis reveals decreased levels of microglial receptor transcripts and pro-inflammatory activation genes in miR^{CD33}-treated *APP/PS1* mice compared to control mice. RNA was extracted from the early intervention mice that were treated with miR control or miR^{CD33} vector. RNA was reverse transcribed and subjected to PCR array that consists of 14 transcripts. Graphs with green bars depict transcripts that were decreased in the miR^{CD33} group compared to control, while graphs with orange bars depict transcripts that were increased in the miR^{CD33} group versus control. *CD33* expression levels were reduced by 33.41% (**$P = 0.0078$) in miR^{CD33}-treated mice compared to control mice. Several microglial receptor transcripts (e.g. *Itgax/CD11c*, *CD47* and *CD36*) and pro-inflammatory activation genes (e.g. *Tlr4* and *Il1b*) were downregulated after miR^{CD33} treatment versus miR control in *APP/PS1* mice. Each symbol in graphs represents an individual animal ($n = 8$ for miR control, $n = 9$ for miR^{CD33}). Data are represented as mean ± SEM.

we found that several microglial receptor transcripts including *Itgax/CD11c* ($P = 0.002$), *CD47* ($P = 0.0243$) and *CD36* ($P = 0.0119$) showed decreased expression in *APP/PS1* mice treated with miR^{CD33} versus miR control (Fig. 5). Non-significant decreases were observed for levels of *Trem2* ($P = 0.3509$) and its adaptor *Tyrobp* ($P = 0.1814$). Interestingly, treatment with miR^{CD33} in *APP/PS1* mice compared to control group led to decreased levels of pro-inflammatory activation genes that included *Tlr4* (31.12% decrease, $P = 0.0469$) and *Il1b* (54.49% decrease, $P = 0.0308$, Fig. 5). The expression levels of the cytokine transcript *Il6* were comparable between the miR^{CD33}-treated and control mice. We observed a large, albeit non-significant reduction in levels of *Ccl2*, the main CCR2 chemokine ligand, (45.70% decrease, $P = 0.1183$) after miR^{CD33} injection in *APP/PS1* mice. We did not observe statistically significant differences in transcript levels of the pro-inflammatory cytokine *Tnf*, anti-inflammatory activation genes, *Arg1* and *Retnla/Fizz1*, or *Apoe* between miR^{CD33}-treated and control mice. In summary, early treatment of *APP/PS1* mice with miR^{CD33} compared to control vector results in reduced expression of microglial receptor genes as well as pro-inflammatory activation genes.

Next, we performed an ELISA specific for the chemokine CCL2 in brain lysates of miR^{CD33} or control treated mice. We also ran a pro-inflammatory panel based on the Meso Scale Discovery multi-spot assay system. We measured simultaneously 10 cytokines and chemokines that are important in neuroinflammatory response and immune system regulation. Some of these proteins (CCL2, TNF-α, IL-1β and IL-6) were also analyzed in the PCR array (Fig. 5).

Levels of CCL2 protein showed a trend toward reduction by 44.58% ($P = 0.059$) in the miR^{CD33} versus control group (Fig. 6). IL-1β was also reduced in the miR^{CD33} group (18.67% decrease, $P = 0.225$), albeit without the statistical significance observed in the PCR array data. Interestingly, TNFα was significantly decreased by 38.48% ($P = 0.0005$) in the miR^{CD33} group at the protein level (Fig. 6), while its levels did not significantly change at the transcript level (Fig. 5). The chemokine CXCL1 (also known as KC/GRO) revealed a trend toward reduced levels (31.3%; $P = 0.075$) in the miR^{CD33} versus control group. The other cytokines analyzed, IL-12p70, IL-5 and IL-6, were minimally changed between the two groups (Fig. 6). Collectively, our cytokine assay data confirm and expand the PCR array results, showing that early injection of miR^{CD33} leads to decreased mRNA or protein levels for the chemokine, CCL2 and pro-inflammatory cytokines, e.g. IL-1β and TNFα, in *APP/PS1* mice.

Discussion

In this study, we utilized a gene therapy approach directly targeting *CD33* in an attempt to reduce neuroinflammation and

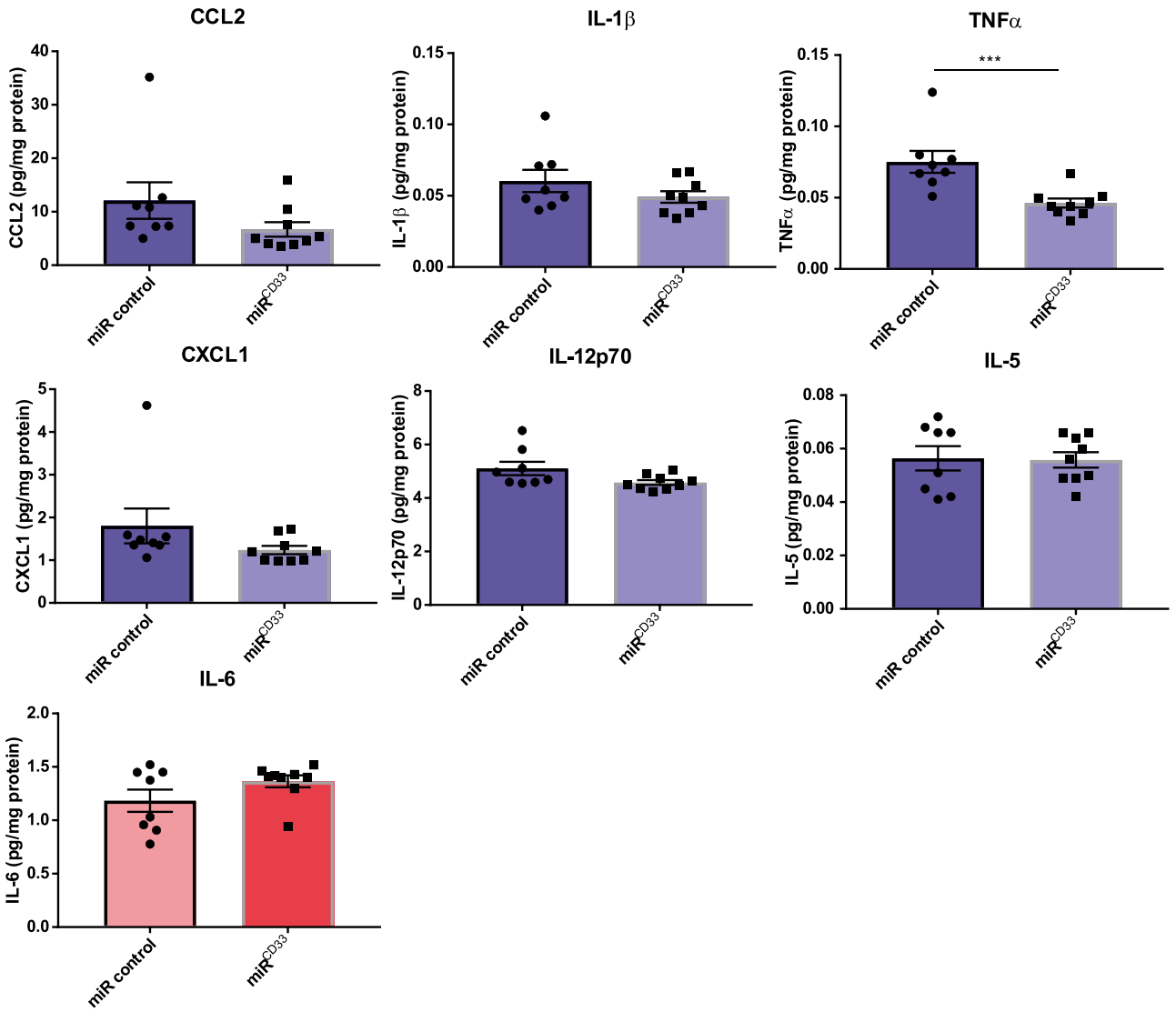

Figure 6. Treatment with miR^{CD33} compared to miR control leads to decreased protein levels of pro-inflammatory cytokines in *APP/PS1* mice. Brain tissue homogenates from the early intervention treated mice were used in a CCL2-specific ELISA and Meso Scale Discovery cytokine assay to detect expression of the indicated proteins. The pro-inflammatory cytokine TNFα was significantly decreased (38.48%, $***P = 0.0005$, Mann–Whitney test) in miR^{CD33}-treated mice compared to control mice. Trends towards reduced levels of chemokines, CCL2 (44.58%, $P = 0.059$) and CXCL1 (31.3%, $P = 0.075$), were observed in miR^{CD33}-treated mice versus control mice. Graphs with blue bars depict transcripts that were decreased in the miR^{CD33} group, while graphs with pink bars depict transcripts that were increased in this group. Each symbol in graphs represents an individual animal ($n = 8$ for miR control, $n = 9$ for miR^{CD33}). Data are represented as mean ± SEM.

Aβ pathology in a mouse model of AD. CD33, a transmembrane protein expressed on the cell surface of microglia, harbors gene variants associated with risk for AD and has been associated with higher levels of Aβ plaque burden (10–13,16). In previous studies, we showed that knockout of *CD33* reduced FA-soluble Aβ42 levels and amyloid plaque burden and attenuated neurodegeneration and improved cognition in mouse models of AD (10,16). These data provided the impetus for developing a therapeutic strategy based on directly targeting CD33 expression, *in vivo*.

AAV vectors have made impressive progress for *in vivo* gene therapy including for treatment of CNS diseases such as spinal muscular atrophy (SMA) in infants (25). Currently, there are two FDA-approved AAV vector-based medicines. The first is a subretinal injection of AAV for the treatment of hereditary blindness (17,26), and the second is a high-dose systemic injection of AAV9 to treat SMA (27) making gene therapies using this vector system translationally viable. However, gene therapy comes with its own challenges, mainly involving dose-related toxicity in some instances and immunogenicity that can either prevent patient treatment in the case of pre-existing anti-AAV antibodies or eliminate transduced cells post dosing, with capsid-specific T cells (28). In recent trials, the use of high-dose glucocorticosteroids has generally managed transient elevation of liver enzymes observed after systemic administration of AAV vectors, and it has been used safely in many treated patients in clinical trials. However in some cases, high systemic doses of AAV (usually those above 10^{14} gc/kg) have resulted in toxicity and death of a non-human primate, which was likely due to systemic inflammation (29). Furthermore, a recent phase I clinical trial using high-dose AAV9 to treat muscular dystrophy was put on hold by the FDA due to an immune reaction in one patient. High

systemic doses are required due to the relatively low efficiency of AAV to provide adequate transgene expression when targeting organs such as the CNS or muscle. However, for CNS targets, the dose, pre-existing antibody levels and systemic toxicity may be mitigated to a certain extent by using either an intrathecal or ICV injection, such as the approach we used in this study. Finally, discovery and engineering of improved viral vectors to deliver therapeutic genes specifically to microglia will lead to better outcomes of gene therapy that is directed towards reducing neuroinflammation such as in AD.

Here, we engineered an AAV vector to encode an artificial miRNA (amiR) targeting *CD33* mRNA. We chose to use amiR over the more traditional shRNA, as it has been reported that the high transduction efficiency of AAV delivering shRNA can lead to neurotoxicity, which is mitigated using miRNA expression cassettes driven by Pol II promoters (30). In this preclinical proof-of-concept study, we also chose to use exosome-enveloped AAV (exo-AAV) as we and others have demonstrated that they are a practical and convenient (from an isolation standpoint) research tool for local and systemic delivery of transgenes to the CNS (22,23,31).

We observed a 30–36% reduction in *CD33* mRNA levels in brain-extracted RNA in both the early and late intervention models. While this reduction was highly significant in the early intervention treatment and resulted in decreased TBS-soluble Aβ levels, amyloid plaque load and neuroinflammatory response, improving the level of *CD33* knockdown will likely increase the therapeutic efficacy of this approach. As AAV9 (and exo-AAV) primarily transduce neurons and astrocytes following direct injection into the brain (22) with some microglia transduction reported (32), it is likely only a small number of microglia were directly transduced by exo-AAV9-miR^{CD33}. We speculate that anti-*CD33* miRs may be exported in various manners from highly transduced neurons and astrocytes and then taken up by microglia, where they target and downregulate *CD33* mRNA. One possible export mechanism of miR^{CD33} could be in the form of extracellular vesicles (aka exosomes), which have been reported to carry an array of molecules including nucleic acids (including miRNAs), proteins and lipids (33,34). Interestingly, a recent study observed that intramuscular injection of an AAV encoding miRs resulted in elevation of those specific miRs in serum exosomes and downregulation of miR targets in kidney cells, which were not transduced by AAV (35). Thus, in some cases, generation of a 'miR factory' in transduced cells by AAV vectors may provide a therapeutic benefit to target cells.

In the future, when AAV variants (whether natural isolates or engineered) are identified that more efficiently transduce microglia directly, our approach should achieve greater efficacy. Furthermore, testing of different miRs or miR clusters targeting different regions of *CD33* may also lead to improved knockdown efficiency.

Adult human and murine microglia are particularly intransigent to AAV transduction. Specificity is another important challenge relevant when transducing microglia because additional cells (mainly neurons and astrocytes) are transduced (36). Therefore, generation of AAVs containing artificial miR^{CD33} driven under a promoter from macrophage lineage (e.g. F4/80, CD68, CD11b and other), which labels monocytes and microglia, could improve microglial transduction *in vivo* (37). Although AAVs are currently the most efficient vector for targeting neurons and astrocytes of the CNS, extensive research is still needed to improve the efficiency and selectivity of *in vivo* transduction in microglia. In addition to transcriptional tailoring with microglial selective promoters, rational engineering of AAVs or the use of AAV capsid libraries to enhance tropism for microglia and cells from the monocyte–macrophage lineage could also improve microglial transduction *in vivo* (38). The rational approach is likely difficult as the rate-limiting steps to transduction of microglia by AAV are currently unknown. Some information may come from studies on other antigen presenting cells such as dendritic cells, where capsid uncoating in the nucleus is proposed to be a rate-limiting step (39).

Both early and late intervention models reduced *CD33* mRNA levels in brain surrounding the injection site; however, early intervention approach is more effective in reducing *CD33* expression. Since the effect of miR^{CD33} on downregulation of *CD33* mRNA levels mostly emerges from a cross-correction from either neurons and/or astrocytes to microglia, a long treatment time is probably needed for the cross-correction to become effective. We found that treatment of *APP/PS1* mice with miR^{CD33} for 2 months (2 months to 4 months of age) did not result in downregulation of *CD33* mRNA levels in comparison to miR control (data not shown). This supports our hypothesis that a long treatment time increases the effects of cross-correction from neurons/astrocytes to microglia and shows that at least a 3-month-long treatment is required to downregulate *CD33* expression.

We also showed that gene therapy approach reduced TBS-soluble Aβ42 for late intervention while reducing TBS-soluble Aβ40 for early intervention model. The difference in reduction of TBS-soluble Aβ species might be due to the timing of therapy (e.g. starting at 2 months of age for early intervention versus 8 months for late intervention). The longer duration of treatment for early intervention (e.g. 2 to 10 months versus 8 to 11 months) might also contribute to a difference in effects on TBS-soluble Aβ40 versus Aβ42. Finally, different ages of *APP/PS1* mice prior to sacrifice (10-month-old for early intervention versus 11-month-old for late intervention) could also be a contributing factor to this difference.

Furthermore, only the early intervention model significantly reduced amyloid plaque load. The early intervention treatment may have been more efficient than later intervention for several reasons. One likely explanation is that early intervention may allow a reduction in the accumulated neuropathology/neuroinflammation over time in the *APP/PS1* mouse model, before pathology is firmly established. In contrast, in the late intervention model, which began gene therapy at 8 months, Aβ plaques have already formed and it may be much more difficult to reduce the higher levels of pathology and neuroinflammation at this stage of disease. Our study suggests that timing of therapy is critical, preferably before excessive amyloid pathology and neuroinflammation in the brain, at which point, rescue of normal microglial function (e.g. clearance of Aβ and apoptotic neurons) and balancing pro- and anti-inflammatory activation of microglia may no longer be feasible. In fact, another recent gene therapy model using AAV encoding a soluble toll-like receptor found that treatment of AD mice at neonatal day P0 greatly reduced Aβ plaque burden by 69%; however, this reduction was only 26% when mice were injected at 9 months of age (40).

We found that knockdown of *CD33* mRNA led to reprogramming of microglial gene expression in *APP/PS1* mice. Treatment with miR^{CD33} compared to miR control resulted in reduced levels of microglial receptor genes (e.g. *Itgax/CD11c*, *CD47* and *CD36*) as well as pro-inflammatory activation genes (e.g. *Tlr4* and *Il1b*) in *APP/PS1* mice. While CD11c has been identified as a potential marker of microglia associated with neurodegenerative diseases (41), another study showed that CD11c-positive microglia exhibited a higher metabolic and lysosomal

activity and expressed immune modulators that limited in flammation (42).

CD47 (also termed integrin associated protein) and CD36 (a class B scavenger receptor) are the constituents of a multicomponent receptor complex of fibrillar Aβ on microglial cell surface (43). Antagonists specific for CD47 and CD36 blocked fibrillar Aβ-stimulated phagocytosis (44). However, another study demonstrated that CD47 expressed on myelin, when reacting to immune inhibitory receptor SIRPα on microglia, reduced myelin phagocytosis by microglial cell cultures (45). Therefore, CD47 can both promote and inhibit phagocytosis, depending on the circumstances.

CD36 is required for phagocytosis of apoptotic cells (46), regulates microglial migration (47) and mediates phagocytosis in post-stroke brains (48). However, upon Aβ binding, CD36 has been reported to form a heterodimeric complex with TLR4 and TLR6 on microglia leading to the production of reactive oxygen species and increased expression of IL-1β (49). Another study suggested that it may be advantageous to inhibit the ability of CD36 to signal when bound to Aβ (50). Thus, downregulation of *CD36* by miR^{CD33} may also be beneficial for lowering levels of reactive oxygen species and the pro-inflammatory cytokine IL-1β.

Following knockdown of *CD33*, only a modest and non-significant decrease was observed in the expression levels of the AD risk factor *TREM2* and its adaptor *TYROBP*. TREM2 is an immunoreceptor expressed on myeloid cells, primarily microglia, where it regulates inflammatory response (51). Our data showing that *CD33* knockdown slightly downregulated *Trem2* levels appears to be in accordance with a previous report that TREM2 expression was increased by the *CD33* AD risk allele rs3865444^{C} and decreased by CD33 immunosuppression (52).

Interestingly, *CD33* knockdown reduced the expression levels of the pro-inflammatory activation genes *Tlr4* and *Il1b*. We also found that the protein levels of the pro-inflammatory cytokine TNFα were decreased in miR^{CD33}-treated mice compared to control mice. TLR4 has been shown to mediate brain injury and inflammation after ischemic stroke (53) and microglial-induced neuronal loss in a three-dimensional human AD model composed of neurons, astrocytes and microglia in a 3D microfluidic platform (54). Finally, pro-inflammatory cytokines, e.g. IL-1β and TNFα, impaired microglial phagocytosis (55). Hence, downregulation of pro-inflammatory activation genes by *CD33* knockdown contributes to reduced amyloid pathology in *APP/PS1* mice.

We also observed a trend toward a reduction in mRNA and protein levels of the chemokine CCL2/MCP-1 in miR^{CD33}-treated mice, as compared to control. CCL2, which is upregulated in human AD brains (56), is mainly expressed by microglia in mouse models of AD (57). Antibodies to CCL2 significantly inhibited the migration of microglia and monocytes in response to Aβ-stimulated macrophage supernatant (58). Neutralizing antibodies against CCL2 also substantially reduced the migration of microglia that proved to be toxic to AD neurons and astrocytes in the human AD triculture system (54). Moreover, miR^{CD33} treatment did not impact the ratio of Iba1-positive or CD68-positive microglia to plaques in *APP/PS1* mice. Although *CD33* knockdown reduces CCL2 levels, it does not impact microglial clustering around plaques, suggesting that additional chemokines might be important for microglial recruitment to plaques in *APP/PS1* mice.

Furthermore, miR^{CD33} treatment resulted in a trend toward decreased protein levels of the chemokine CXCL1, which is expressed in endothelial cells, microglia, neurons and astrocytes (59), and is a key regulator of granulocyte recruitment into the CNS (60). Monocytes derived from AD patients expressed high levels of CXCL1, which contributed to Aβ-induced transendothelial (blood–brain barrier traversing) migration of monocytes in AD (61). Administration of anti-CXCL1 antibodies decreased the severity of experimental autoimmune encephalitis (60). Our data showing that miR^{CD33} treatment reduces CXCL1 levels suggest that CD33 might impact the chemotactic response originating not only from microglia but also from other brain cells as well. Thus, reducing CXCL1 levels via *CD33* knockdown could be beneficial for the treatment of neuroinflammation.

In conclusion, we demonstrate that specifically targeting the message of *CD33*, an AD risk gene, by using an AAV vector encoding artificial miRNA, can significantly reduce Aβ pathology and neuroinflammation in a mouse model of AD. Future optimization of this technology, e.g. at the level of AAV efficiency for microglial transduction, and translation into clinical treatment modalities, may yield a potent new therapy for the treatment and prevention of AD.

Materials and Methods

Construction of AAV vector encoding artificial miRNA targeting CD33.

We used a similar strategy to Stoica *et al.* (18) to generate an artificial miRNA (amiR) targeting CD33. We used the miR-155 flanking and loop sequences described in Invitrogen's Block-iT™ Pol II miR RNAi Expression Vector Kits manual (Thermo Fisher), which is based on technology developed by David Turner's laboratory (US Patent Publication No. 2004/00053876). Briefly, we used Invitrogen's Block-iT miR RNAi designer software by inputting the cDNA sequence for mouse *CD33* (isoform 1, NCBI Reference Sequence: NM_001111058.1). We selected the top predicted mature miR (anti-sense) sequence to target murine *CD33* mRNA. This sequence was 5'TAGAGAGGTCACATGCAGTGA3'. This miR binds to nucleotides 480–500 in the transcript, which spans exon 2 and exon 3. The miR^{CD33} also binds to nucleotides 480–500 in mouse *CD33* isoform 2 (NCBI Reference Sequence: NM_021293.3). Finally, miR^{CD33} binds at positions 411–431 and 410–430 in mouse *CD33* isoforms, NM_021293.1 and NM_021293.2, respectively.

We designed sense and anti-sense overlapping oligos encoding the entire miR-155 backbone with *CD33* specific miR (miR^{CD33}) with XbaI flanking overhangs. We also designed oligos for miR control (from Invitrogen BlockiT manual) with antisense sequence: 5'GAAATGTACTGCGCGTGGAGAC3'. The miR control, according to the manufacturer's manual, is composed of a sequence that makes a proper hairpin that gets processed into a mature miRNA. However, the sequence is not predicted to recognize any mammalian vertebrate mRNAs.

miR^{CD33} top oligo:
5'CTAGATGCTGTAGAGAGGTCACATGCAGTGAGTTTTGGCCAC
TGACTGACGACTCACTGCATGACCTCTCTACAGGT3'.
miR^{CD33} bottom oligo:
5'CTAGACCTGTAGAGAGGTCATGCAGTGAGTCGTCAGTCAGTG
GCCAAAACTCACTGCATGTGACCTCTCTACAGCAT3'.
miR control top oligo:
5'CTAGATGCTGGAAATGTACTGCGCGTGGAGACGTTTTGGCC
ACTGACTGACGTCTCCACGCAGTACATTTCAGGT3'.
miR control bottom oligo:
5'CTAGACCTGAAATGTACTGCGTGGAGACGTCAGTCAGTGGC
CAAAACGTCTCCACGCGCAGTACATTTCCAGCAT3'.

Oligos were annealed and the DNAs encoding the miRs were cloned into an AAV expression plasmid, AAV-CBA-GFP-WPRE. When packaged into AAV capsid, this plasmid encodes a single stranded vector genome. The promoter is a hybrid CMV immediate early/CBA promoter driving GFP, followed by a

woodchuck posttranscriptional regulatory element (WPRE) and tandem bovine growth hormone and SV40 polyA signal sequences. The annealed overlapping oligos were ligated with AAV-CBA-GFP-WPRE, digested with XbaI located between GFP and WPRE sequences. Next, we sequenced the cloned plasmids for verification of correct orientation of the insert. This generated the following two AAV plasmids: AAV- miR^{CD33} and AAV-miR control.

exo-AAV preparations. exo-AAV were produced in 293T cells as previously described (21). Briefly, a triple transfection of AAV plasmid, rep/cap plasmid (AAV9 serotype used) and helper plasmids was performed using the calcium phosphate method in ten 15-cm dishes. Media was changed to 2% fetal bovine serum (FBS) in Dulbecco's modified Eagle's media (DMEM) the day after transfection and to exosomes-free 2% FBS at 48 h post transfection. At 72 h post transfection, media was harvested. Cell debris and apoptotic bodies were removed by sequential, 10 minutes 300× g and 2000× g centrifugations, respectively. The supernatant containing exo-AAV was then centrifuged at 20000× g for 1 hour to deplete larger microvesicles. Next, the remaining media was centrifuged at 100000× g for 1 hour using a Type 70 Ti rotor in an Optima™ L-90 K ultracentrifuge (both Beckman Coulter, Inc., Indianapolis IN). The resulting pelleted material was resuspended in serum-free, antibiotic-free DMEM. exo-AAV preparations were stored at −80°C until use. Before titration, exo-AAV sample was treated with DNase to remove plasmid DNA from the transfection by mixing 5 µl of the sample with 1-µl DNase I, 5-µl 10× buffer and 39-µl water. Samples were incubated for 1 hour at 37°C and then DNase I was inactivated at 75°C for 15 minutes. We purified AAV genomes using High Pure Viral Nucleic Acid Kit (Roche, Indianapolis, IN). Next, exo-AAV preparations were titered using a quantitative TaqMan PCR that detects AAV genomes (polyA region of the transgene cassette), as previously described (22).

HEK293T stably expressing murine CD33. To test knockdown of murine *CD33* (m*CD33*) in cell culture, we generated HEK293T cells transduced by a lentivirus vector encoding m*CD33*. The cDNA encoding m*CD33* was PCR amplified from the plasmid m*CD33* (NM_001111058.1, cat # MC208244, OriGene) using Phusion polymerase (NEB) and the following primers: for cd33 NheI ATAGCTAGCGCCACCATGCTGTGGCCACTG and Rev cd33 XhoI ATTAGCTCGAGTCAACTGAGTGTAAGACTCAC. The primers contain flanking NheI and XhoI restriction sites facilitating ligation into similarly digested lentivirus plasmid CSCW2 (citation). This plasmid drives expression of the cDNA (i.e. m*CD33*) under the CMV promoter. It also contains an internal ribosomal entry site (IRES), which allows for expression of mCherry fluorescent protein. We call this plasmid CSCW2-CMV-mCD33-IRES-mCherry. VSV-G pseudotyped lentivirus, lenti-CMV-mCD33-IRES-mCherry, was produced by the MGH Vector Core. Next, to generate HEK239T cells stably expressing mCD33, a well of a six-well plate containing ∼5×10^5 cells was incubated with 100 µl of the vector preparation diluted in a total volume of 1 ml of DMEM containing 10% FBS. The following day the media was changed, and cells were passaged. Four days post transduction cells were examined for mCherry fluorescence and approximately 80% of cells expressed mCherry at varying fluorescence intensity.

Next, to isolate a clonal population of cells with low levels of mCD33 (at levels similar to those of microglia), we trypsinized and centrifuged HEK293T cells expressing lenti-CMV-mCD33-IRES-mCherry. Cells were washed with phosphate buffer saline (PBS) and centrifuged. The cell pellet was resuspended in FACS sorting buffer consisting of 2% heat-inactivated fetal bovine serum, 2% B27 supplement (cat # 17504-044, Gibco) in PBS. Single cells were FACS-sorted based on low expression levels of the mCherry fluorescent protein (PE-Texas red channel), using FACS ARIA (BD Biosciences). Single cells were sorted into 96-well plates containing cell growth media: DMEM (cat # 12-604F, Lonza), 10% heat-inactivated fetal bovine serum, 2 mM L-glutamine and 1% penicillin/streptomycin (Life Technologies). After 1 week, half of the cell growth media was replaced with fresh media in each well every 3 days. After an additional week, each single cell clone was trypsinized and transferred into one well in 24-well plates for cell expansion. Upon reaching confluency, each single cell clone was trypsinized and plated into two wells in six-well plates. Once confluent, cells from one well were frozen in heat-inactivated fetal bovine serum containing 10% dimethyl sulfoxide (cat # D2650, Sigma Aldrich), while cells in the second well were lysed in RNA lysis buffer (RLT-Plus, cat # 1053393, Qiagen) containing 1% β-mercaptoethanol (cat # 63689, Sigma Aldrich). We obtained 32 single cell clones expressing mCD33 and screened them for the lowest expression levels of mouse *CD33* transcript by using qPCR.

RNA was isolated from resulting cell lysates using the RNeasy Mini Kit (cat # 74104, Qiagen) according to the manufacturer's instructions. During RNA extraction, samples were treated with RNase-free DNase I (cat # 79254, Qiagen) directly on the RNeasy spin columns at room temperature (RT) for 15 minutes and washed with buffer RW1 (Qiagen). Each RNA sample was eluted in RNase-free water (50 µl). Purified RNA was quantified using Qubit RNA Broad Range Assay Kit (cat # Q10211, Thermo Fisher Scientific) on the Qubit Fluorometer 3.0 (Thermo Fisher Scientific). RNA (800 ng) was reverse-transcribed using the SuperScript III First Strand Synthesis System and oligo-DT (20) primer (cat # 18080–051, Invitrogen). Gene expression was assessed by performing TaqMan real-time PCR assays. The probe targeting the mouse *CD33* gene was labeled with FAM (Mm00491152_m1 specific to exon boundary 3–4, Thermo Fisher Scientific). The housekeeping human *GAPDH* gene was used as control, and the probe targeting *GAPDH* was labeled with VIC (Hs02786624_g1 specific to exon 7 or 8, Thermo Fisher Scientific). 1:10 diluted cDNAs were mixed with the probes and Taqman Universal Master Mix II (cat # 4440038, Applied Biosystems) and amplified using the C1000 Touch Thermal Cycler (Bio-Rad). Results were analyzed by the comparative CT method. Average CT values for each sample were normalized to the average CT values of the housekeeping gene. Finally, the single cell clone line expressing the lowest mouse *CD33* transcript levels was identified. The corresponding frozen cell vial was rapidly thawed and plated in cell growth media in a 10-cm culture dish to allow cell expansion.

Knockdown of mCD33 mRNA in a single cell clone HEK293T-mCD33 line. Cells were plated at a density of 7×10^5 cells/well in six-well tissue culture plates. The following day, cells were transfected via the calcium phosphate method with 2 µg of either the AAV-miR^{CD33} and AAV-miR control plasmids ($n = 6$/group). The next day, cell growth media was changed. This transfection results in >90% transfection efficiency observed by the IRES-driven GFP cassette in the plasmid. Seventy-two hours post-transfection, cells were washed with PBS and lysed in RNA lysis buffer containing 1% β-mercaptoethanol. RNA was isolated from cell lysates, quantified and reverse transcribed, as described

above. Gene expression was assessed by performing TaqMan real-time PCR assays, as described above. The probe targeting the mouse *CD33* gene was labeled with FAM (Mm00491152_m1 specific to exon boundary 3–4, Thermo Fisher Scientific). The housekeeping human *GAPDH* gene was used as control and the probe targeting *GAPDH* was labeled with VIC (Hs02786624_g1 specific to exon 7 or 8, Thermo Fisher Scientific). Results were analyzed by the comparative CT method. Average CT values for each sample were normalized to the average CT values of the housekeeping gene. Finally, the results were normalized to the mean of the miR control group.

Mice. All animal experiments were approved by the Massachusetts General Hospital Subcommittee on Research Animal Care following guidelines set forth by the National Institutes of Health Guide for the Care and Use of Laboratory Animals. For all experiments we used B6C3 Tg(APPswe, PSEN1dE9)85Dbo/Mmjax (MMRRC stock number: 34829-JAX) female mice from the Jackson laboratory (Bar Harbor, ME). We used only female *APP/PS1* mice due to the variance in Aβ42 levels between males and females. In addition, we have previously reported that AAV9 transduces brain in females with a higher efficiency as compared to males when injected intravenously (62). While we delivered the vector through the lateral ventricles in the present study, and AAV transduction based on sex after this route is unknown, we wanted to minimize the variability in transduction that this could cause.

Intracerebroventricular injections. Injections into both lateral ventricles were performed using the following coordinates AP: −0.4, ML: +1.0, DV: −1.7 for left ventricle and AP: −0.4, ML: −1.0, DV: −1.7 for right ventricle. Five microliters of vector (dose in genome copies indicated in results section and below) were infused into each ventricle at a rate of 1 µl/min using a microinjector (World Precision Instruments) fitted with a 30 gauge needle attached to a 10 µl gas-tight syringe (Hamilton). The needle was left in place for 2 minutes post injection before slowly withdrawing.

Late intervention therapy. APP/PS1 mice were injected with vector (8×10^{10} GC) at 8 months of age and sacrificed at 11 months of age.

Early intervention therapy. APP/PS1 mice were injected with vector (7.5×10^{10} GC) at 2 months of age and sacrificed at 10 months of age.

Immunostaining of brain cryosections. Mice were euthanized by ketamine/xylazine overdose and brain tissue collected for post-mortem analyses. One hemisphere was used for immunohistochemistry. After cryoprotection of the brain in 30% glycerol for 48 hours, 40 µm-thick floating sections were cut on a freezing microtome in the coronal plane. Floating sections were permeabilized in 0.5% triton in TBS for 30 minutes, blocked in 5% normal goat serum (NGS) in TBS for 1 hour, and incubated with primary antibody at 1:500 overnight at 4°C in 2.5% NGS and 0.1% Triton X-100 in TBS. Primary antibodies used for this study were chicken polyclonal anti-GFP (cat # GFP-1020, Aves Labs, Tigard, USA), rabbit polyclonal anti-Aβ (N-terminal) (cat # 18584, IBL/Tecan, USA), rabbit polyclonal anti-Iba1 (cat # 019–19 741, Wako, Japan), rat monoclonal anti-CD68 antibody (cat # MCA1957GA, clone FA-11, Bio-Rad, USA), mouse monoclonal anti-NeuN (cat # MAB377, EMD Millipore, Burlington, MA, USA) and rabbit polyclonal anti-glutamine synthetase (cat # ab49873, Abcam, Cambridge, MA, USA). Sections were then washed with TBS and incubated with appropriate Alexa-Fluor 488 or Alexa-Fluor 568 conjugated secondary antibodies diluted at 1:1000 in 2.5% NGS and 0.1% Triton X-100 in TBS. After another round of washing, sections were mounted onto slides and coverslipped with Vectashield mounting medium with DAPI (Vector Labs). For the counterstaining of amyloid with Methoxy-XO4 (after staining for CD68 or Iba1), the floating sections were incubated for 15 minutes in a solution of 1 µg/ml of Methoxy-XO4 (diluted in TBS) before mounting the slices with Fluoromount-G (No DAPI, SouthernBiotech).

CD33 RT-qPCR on mouse brain tissue

From one hemisphere we extracted two 1-mm slices of brain spanning the ventricles (injection site). One of the two brain slices was used for RNA extraction. RNA was isolated from brain tissue with Trizol (cat # 15596–026, Invitrogen), following the manufacturer's protocol. The RNA pellet was washed with 75% ethanol, air-dried and resuspended in water. The RNA was reverse-transcribed using the SuperScript III First Strand Synthesis System and oligo-DT (20) primer (cat # 18080–051, Invitrogen). Gene expression was assessed by performing TaqMan real-time PCR assays. The probe targeting the mouse *CD33* gene was labeled with FAM (Mm00491152_m1 specific to exon boundary 3–4, Thermo Fisher Scientific). The housekeeping mouse *GAPDH* gene was used as control, and the probe targeting *GAPDH* was labeled with VIC (Mm99999915_g1 specific to exon boundary 2–3, Thermo Fisher Scientific). 1:10 diluted cDNAs were mixed with the probes and Taqman Universal Master Mix II (cat # 4440038, Applied Biosystems) and amplified using the C1000 Touch Thermal Cycler (Bio-Rad). Results were analyzed by the comparative CT method. Average CT values for each sample were normalized to the average CT values of the housekeeping gene. Finally, the results were normalized to the mean of the control group (miR control injected mice).

Amyloid beta quantitation: Meso Scale Discovery multi-spot assay system

From one hemisphere we extracted two 1 mm slices of brain spanning the injection site. One of the two brain slices was used for quantitation of Aβ levels. Brain tissue was homogenized in 5 volumes of tissue homogenization buffer that contains 25 mM Tris–HCl at pH 7.4, 130 mM NaCl, 2.7 mM KCl, 5 mM EDTA, phosphatase inhibitor (Thermo Fisher Scientific, cat # 1862495), EDTA-free protease inhibitor cocktail (Roche, cat # 11873580001) and 2 mM 1,10-phenantroline (Sigma Aldrich, cat # 1313777) at 4°C. The homogenates were centrifuged at 18000 g for 30 minutes at 4°C, using a Microfuge 18 Centrifuge (Beckman Coulter). Supernatants were collected and used to measure TBS-soluble Aβ. The pellet was extracted in 70% formic acid (FA, equal volume of TBS) with a hand homogenizer (Wheaton) on ice. Samples were centrifuged at 100000 g for 1 hour at 4°C, using an Optima TL ultracentrifuge and a TLA 120.2 rotor (Beckman Coulter). FA supernatants were collected, neutralized with 1 M Tris-base, pH 11 (1:17 v:v) and used to measure FA-soluble Aβ. TBS-soluble and FA-soluble Aβ levels were measured by an electrochemiluminescence-based multi-array method on the platform of the MESO Quickplex SQ 120 system (by Meso Scale Diagnostics, LLC). The V-PLEX Aβ Peptide Panel 1 (4G8) Kit (cat # K15199E, Meso Scale Discovery) was utilized to detect simultaneously the Aβ38, Aβ40 and Aβ42 peptides in a 96-well multi-spot assay system, following manufacturer's instructions. The electrochemi-luminescence signals for all samples were

captured by the Quickplex SQ 120 system and analyzed using the Meso Scale Discovery standards and software. TBS-soluble Aβ levels were further normalized to sample total protein concentrations. TBS-soluble lysates were assessed for total protein concentrations using the BCA Protein Assay Reagents A and B (cat # 23223 and 23 224, Pierce).

Amyloid beta quantitation: Human/Rat β Amyloid ELISAs

In some experiments for the TBS-soluble lysates, we used ELISA to detect Aβ40 and Aβ42 levels. We used the Human/Rat β Amyloid (40) ELISA Kit Wako II, BNT77/BA27(Fab') (cat # 294–64 701, Wako) and the Human/Rat β Amyloid (42) ELISA Kit Wako High-Sensitive, BNT77/BC05 (Fab'), (cat # 292–64 501, Wako).

Western blot analysis. Brain tissue was homogenized in 5 volumes of tissue homogenization buffer that contains 25 mM Tris–HCl at pH 7.4, 130 mM NaCl, 2.7 mM KCl, 5 mM EDTA, phosphatase inhibitor (cat # 1862495, Thermo Fisher Scientific), EDTA-free protease inhibitor cocktail (cat # 11873580001, Roche) and 2 mM 1,10-phenantroline (cat # 1313777, Sigma Aldrich) at 4°C. The homogenates were centrifuged at 18000 g for 30 minutes at 4°C, using a Microfuge 18 Centrifuge (Beckman Coulter). Supernatants were collected and mixed with 10× radio-immunoprecipitation assay buffer (1:10 v:v; cat # 20–188, EMD Millipore) supplemented with all the above-described inhibitors. Samples were incubated on a rotating wheel for 30 minutes at 4°C and centrifuged at 12000 g for 15 minutes at 4°C. The supernatant was collected and used for western blotting. Lysates were assessed for protein concentration using the BCA Protein Assay (cat # 23223 and 23 224, Pierce). Samples were boiled in sample buffer (NuPAGE, cat # NP0007, Life Technologies) containing lithium dodecyl sulfate and β-mercaptoethanol as reducing agent and resolved on 4%–12% Bis-Tris polyacrylamide precast gels (NuPAGE system, cat # NP0321BOX, Life Technologies). Gels were transferred onto PVDF membranes (cat # 162–0177, BioRad) using wet transfer system (BioRad). Western blots were blocked in 0.1% Tween-20 with 5% w/v non-fat dry milk in TBS for 1 hour at RT. The primary antibody was directed against human APP (1:1000, rabbit polyclonal, clone C7 targeting the amino acid residues 732–751 in APP, custom-designed by Open Biosystems) and was incubated overnight in 0.1% Tween-20 with 5% milk in TBS at 4°C. Western blots were incubated with goat anti-rabbit-HRP antibody (1:6000; cat # A0545, Sigma-Aldrich) in 0.1% Tween-20 with 3% milk in TBS for 1 hour at RT. Signal was detected using the Prometheus ProSignal Dura chemiluminescent substrate (cat # 20–301, Genesee Scientific). For GAPDH detection, western blots were blocked with Odyssey Blocking Buffer (TBS, cat # 927–50 000, LI-COR) for 1 hour at RT and incubated with anti-GAPDH antibody (1:3000, mouse monoclonal, cat # MAB374, EMD Millipore) in Odyssey Blocking Buffer overnight at 4°C. Western blots were incubated with IRDye 800CW donkey anti-mouse antibody (1:6000, cat # 926–32 212, LI-COR) in Odyssey Blocking Buffer for 1 hour at RT. Finally, western blots were imaged with Odyssey FC and densitometric analyses were performed with Imaging Studio (LI-COR Biosciences). Density values of APP, α-CTF and β-CTF bands were normalized to GAPDH levels.

Stereology-based quantification of amyloid, Iba1 and CD68 load in the cortex and hippocampus. Stereology-based studies of amyloid, CD68 and Iba1 loads were performed after scanning all the slides using the batch mode function of the Olympus VS120 epifluorescence microscope under a ×20 objective (Numerical Aperture 1.2). For each channel, the exposure time remained unchanged during image acquisition and analysis. Image analysis was done with the Olympus CellSens software. The cortex and hippocampus were outlined, and a fixed threshold was applied for each channel to allow automatic detection of amyloid plaques (either after staining for amyloid by immunohistology or by Methoxy-XO_4), CD68-positive and Iba1-positive microglia. The density of amyloid deposits and amyloid load were calculated by reporting the total number of amyloid plaques or the total area occupied by amyloid to the surface of cortex or hippocampus. The load of CD68 and Iba1-positive microglia was determined by calculating the ratio of the area occupied by each microglial marker to the total area of amyloid (stained by the dye Methoxy-XO4) within the same brain region of interest (either cortex or hippocampus). The results were normalized to the mean of the control group (miR control injected mice). All stereology quantification was carried out blinded until the last statistical analyses.

Custom Taqman Array Plate. We used the Taqman® Array Plates Fast 96-Well Plates (Life Technologies) to assay the following transcripts: *GAPDH* (housekeeping), *CD33*, *CD11c*, *Trem2*, *Tyrobp*, *Arg1*, *Fizz1*, *Ccl2*, *Il1b*, *Il6*, *Tnf*, *Tlr4*, *CD47*, *CD36* and *Apoe*. We used cDNA prepared from whole-brain extracts spanning the injection site described above. We followed the manufacturer's instructions and performed the qPCR in an ABI 7500 Fast qPCR machine (Applied Biosystems). All transcript levels were normalized to *GAPDH* using the ΔCt method. Fold differences between the miR control and miR^{CD33} groups were calculated using the $2^{-\Delta\Delta Ct}$ method.

CCL2 ELISA

TBS-soluble fractions from mouse brain tissue (spanning the injection site) were generated as described in the Aβ quantitation section. CCL2 protein levels were assessed in TBS-soluble fractions using the Mouse CCL2/JE/MCP-1 Quantikine ELISA Kit (cat # MJE00B, R&D Systems) and following the manufacturer's protocol. The colorimetric signals of all samples were captured using the Synergy 2 microplate reader (BioTek Instruments) and analyzed using the CCL2/MCP-1 standard provided in the Quantikine ELISA Kit. CCL2 expression levels were normalized to total protein concentrations that were determined by BCA Protein Assay (cat # 23223 and 23 224, Pierce).

Meso Scale Discovery Multi-Spot Cytokine Assay

TBS-soluble fractions from mouse brain tissue (spanning the injection site) were generated as described in the Aβ quantitation section. Expression levels of 10 cytokines and chemokines were measured in TBS-soluble fractions using an electrochemiluminescence-based multi-array method on the platform of the MESO Quickplex SQ 120 system. The V-PLEX Proinflammatory Mouse 1 Kit (cat # K15048D, Meso Scale Discovery) was utilized to detect simultaneously the IFN-γ, IL-1β, IL-2, IL-4, IL-5, IL-6, CXCL1/KC/GRO, IL-10, IL-12p70 and TNF-α cytokines in a 96-well multi-spot assay system, following manufacturer's protocol. The electrochemiluminescence signals for all samples were captured by the Quickplex SQ 120 system and analyzed using the standards and software provided by the manufacturer. Robust signals were obtained for all samples for IL-1β, IL-5, IL-6, CXCL1/KC/GRO, IL-12p70 and TNF-α. Cytokine expression levels were normalized

to sample total protein concentrations that were assessed using the BCA Protein Assay (cat # 23223 and 23 224, Pierce).

Quantification and statistical analysis

Statistical analysis was performed using the GraphPad Prism 7 (GraphPad Software). The normality of data sets was tested with the D'Agostino-Pearson omnibus test. Unpaired *t* test with Welch's correction was performed for normally distributed data sets and Mann–Whitney test otherwise. Data collection and analysis were blindly performed. All *n* and *P*-values and statistical tests are indicated in the Results section and figure legends.

Supplementary Material

Supplementary Material is available at *HMG* online.

Acknowledgements

We thank the MGH Quantitative Real-Time PCR Core Facility for use of the quantitative PCR equipment for AAV quantitation and RT-qPCR.

Conflict of Interest statement. C.A.M. has issued as well as pending patent applications involving the exo-AAV platform. C.A.M. has a financial interest in Chameleon Biosciences, Inc., a company developing an enveloped adeno-associated virus vector platform technology for repeated dosing of systemic gene therapy. C.A.M.'s interests were reviewed and are managed by the Massachusetts General Hospital and Partners HealthCare in accordance with their conflict of interest policies. A.G. and R.E.T. have an issued patent on gene therapy for neuroinflammation using *CD33*.

Funding

Cure Alzheimer's Fund Award (to C.A.M., E.H., A.G. and R.E.T.); Partners Healthcare Innovation Discovery Grant (to C.A.M.); National Institute on Aging/National Institutes of Health (5R00AG049056 to A.G., 1R00AG047336-01A1 to E.H.); The JPB Foundation (to R.E.T.).

Author Contributions

A.G., C.A.M., E.H. and R.E.T. conceived of the study, carried out experiments, analyzed data and wrote the manuscript.

J.N. and E.P.L. carried out experiments and analyzed data.

A.M.F., A.N.F., D.M., H.N., A.V., S.L. and S.G. carried out experiments.

References

1. Gatz, M., Reynolds, C.A., Fratiglioni, L., Johansson, B., Mortimer, J.A., Berg, S., Fiske, A. and Pedersen, N.L. (2006) Role of genes and environments for explaining Alzheimer disease. *Arch. Gen. Psychiatry*, **63**, 168–174.
2. Tanzi, R.E. (2012) The genetics of Alzheimer disease. *Cold Spring Harb. Perspect. Med.*, **2**, a006296.
3. Chapuis, J., Hansmannel, F., Gistelinck, M., Mounier, A., Van Cauwenberghe, C., Kolen, K.V., Geller, F., Sottejeau, Y., Harold, D., Dourlen, P. *et al.* (2013) Increased expression of BIN1 mediates Alzheimer genetic risk by modulating tau pathology. *Mol. Psychiatry*, **18**, 1225–1234.
4. Lambert, J.C., Ibrahim-Verbaas, C.A., Harold, D., Naj, A.C., Sims, R., Bellenguez, C., DeStafano, A.L., Bis, J.C., Beecham, G.W., Grenier-Boley, B. *et al.* (2013) Meta-analysis of 74,046 individuals identifies 11 new susceptibility loci for Alzheimer's disease. *Nat. Genet.*, **45**, 1452–1458.
5. Bertram, L., Lange, C., Mullin, K., Parkinson, M., Hsiao, M., Hogan, M.F., Schjeide, B.M., Hooli, B., Divito, J., Ionita, I. *et al.* (2008) Genome-wide association analysis reveals putative Alzheimer's disease susceptibility loci in addition to APOE. *Am. J. Hum. Genet.*, **83**, 623–632.
6. Efthymiou, A.G. and Goate, A.M. (2017) Late onset Alzheimer's disease genetics implicates microglial pathways in disease risk. *Mol. Neurodegener.*, **12**, 43.
7. Hollingworth, P., Harold, D., Sims, R., Gerrish, A., Lambert, J.C., Carrasquillo, M.M., Abraham, R., Hamshere, M.L., Pahwa, J.S., Moskvina, V. *et al.* (2011) Common variants at ABCA7, MS4A6A/MS4A4E, EPHA1, CD33 and CD2AP are associated with Alzheimer's disease. *Nat. Genet.*, **43**, 429–435.
8. Naj, A.C., Jun, G., Beecham, G.W., Wang, L.S., Vardarajan, B.N., Buros, J., Gallins, P.J., Buxbaum, J.D., Jarvik, G.P., Crane, P.K. *et al.* (2011) Common variants at MS4A4/MS4A6E, CD2AP, CD33 and EPHA1 are associated with late-onset Alzheimer's disease. *Nat. Genet.*, **43**, 436–441.
9. Pillai, S., Netravali, I.A., Cariappa, A. and Mattoo, H. (2012) Siglecs and immune regulation. *Annu. Rev. Immunol.*, **30**, 357–392.
10. Griciuc, A., Serrano-Pozo, A., Parrado, A.R., Lesinski, A.N., Asselin, C.N., Mullin, K., Hooli, B., Choi, S.H., Hyman, B.T. and Tanzi, R.E. (2013) Alzheimer's disease risk gene CD33 inhibits microglial uptake of amyloid beta. *Neuron*, **78**, 631–643.
11. Karch, C.M., Jeng, A.T., Nowotny, P., Cady, J., Cruchaga, C. and Goate, A.M. (2012) Expression of novel Alzheimer's disease risk genes in control and Alzheimer's disease brains. *PLoS One*, **7**, e50976.
12. Walker, D.G., Whetzel, A.M., Serrano, G., Sue, L.I., Beach, T.G. and Lue, L.F. (2015) Association of CD33 polymorphism rs3865444 with Alzheimer's disease pathology and CD33 expression in human cerebral cortex. *Neurobiol. Aging*, **36**, 571–582.
13. Bradshaw, E.M., Chibnik, L.B., Keenan, B.T., Ottoboni, L., Raj, T., Tang, A., Rosenkrantz, L.L., Imboywa, S., Lee, M., Von Korff, A. *et al.* (2013) CD33 Alzheimer's disease locus: altered monocyte function and amyloid biology. *Nat. Neurosci.*, **16**, 848–850.
14. Malik, M., Chiles, J., 3rd, Xi, H.S., Medway, C., Simpson, J., Potluri, S., Howard, D., Liang, Y., Paumi, C.M., Mukherjee, S. *et al.* (2015) Genetics of CD33 in Alzheimer's disease and acute myeloid leukemia. *Hum. Mol. Genet.*, **24**, 3557–3570.
15. Malik, M., Simpson, J.F., Parikh, I., Wilfred, B.R., Fardo, D.W., Nelson, P.T. and Estus, S. (2013) CD33 Alzheimer's risk-altering polymorphism, CD33 expression, and exon 2 splicing. *J. Neurosci.*, **33**, 13320–13325.
16. Griciuc, A., Patel, S., Federico, A.N., Choi, S.H., Innes, B.J., Oram, M.K., Cereghetti, G., McGinty, D., Anselmo, A., Sadreyev, R.I. *et al.* (2019) TREM2 acts downstream of CD33 in modulating microglial pathology in Alzheimer's disease. *Neuron*, **103**, 820–835 e827.
17. McGinley, L. (2017) *The Washington Post*, in press.
18. Stoica, L. and Sena-Esteves, M. (2016) Adeno associated viral vector delivered RNAi for gene therapy of SOD1 amyotrophic lateral sclerosis. *Front. Mol. Neurosci.*, **9**, 56.
19. Gyorgy, B., Fitzpatrick, Z., Crommentuijn, M.H., Mu, D. and Maguire, C.A. (2014) Naturally enveloped AAV vectors for

shielding neutralizing antibodies and robust gene delivery in vivo. *Biomaterials*, **35**, 7598–7609.
20. Schiller, L.T., Lemus-Diaz, N., Rinaldi Ferreira, R., Boker, K.O. and Gruber, J. (2018) Enhanced production of exosome-associated AAV by overexpression of the tetraspanin CD9. *Mol. Ther. Methods Clin. Dev.*, **9**, 278–287.
21. Meliani, A., Boisgerault, F., Fitzpatrick, Z., Marmier, S., Leborgne, C., Collaud, F., Simon Sola, M., Charles, S., Ronzitti, G., Vignaud, A. *et al.* (2017) Enhanced liver gene transfer and evasion of preexisting humoral immunity with exosome-enveloped AAV vectors. *Blood Adv.*, **1**, 2019–2031.
22. Hudry, E., Martin, C., Gandhi, S., Gyorgy, B., Scheffer, D.I., Mu, D., Merkel, S.F., Mingozzi, F., Fitzpatrick, Z., Dimant, H. *et al.* (2016) Exosome-associated AAV vector as a robust and convenient neuroscience tool. *Gene Ther.*, **23**, 380–392.
23. Orefice, N.S., Souchet, B., Braudeau, J., Alves, S., Piguet, F., Collaud, F., Ronzitti, G., Tada, S., Hantraye, P., Mingozzi, F. *et al.* (2019) Real-time monitoring of exosome enveloped-AAV spreading by endomicroscopy approach: a new tool for gene delivery in the brain. *Mol. Ther. Methods Clin. Dev.*, **14**, 237–251.
24. Hanlon, K.S., Meltzer, J.C., Buzhdygan, T., Cheng, M.J., Sena-Esteves, M., Bennett, R.E., Sullivan, T.P., Razmpour, R., Gong, Y., Ng, C. *et al.* (2019) Selection of an efficient AAV vector for robust CNS transgene expression. *Mol. Ther. Methods Clin. Dev.*, **15**, 320–332.
25. Mendell, J.R., Al-Zaidy, S., Shell, R., Arnold, W.D., Rodino-Klapac, L.R., Prior, T.W., Lowes, L., Alfano, L., Berry, K., Church, K. *et al.* (2017) Single-dose gene-replacement therapy for spinal muscular atrophy. *N. Engl. J. Med.*, **377**, 1713–1722.
26. Gruntman, A.M. and Flotte, T.R. (2018) The rapidly evolving state of gene therapy. *FASEB J.*, **32**, 1733–1740.
27. Al-Zaidy, S.A. and Mendell, J.R. (2019) From clinical trials to clinical practice: practical considerations for gene replacement therapy in SMA type 1. *Pediatr. Neurol.*, **100**, 3–11.
28. Manno, C.S., Pierce, G.F., Arruda, V.R., Glader, B., Ragni, M., Rasko, J.J., Ozelo, M.C., Hoots, K., Blatt, P., Konkle, B. *et al.* (2006) Successful transduction of liver in hemophilia by AAV-factor IX and limitations imposed by the host immune response. *Nat. Med.*, **12**, 342–347.
29. Hinderer, C., Katz, N., Buza, E.L., Dyer, C., Goode, T., Bell, P., Richman, L.K. and Wilson, J.M. (2018) Severe toxicity in nonhuman primates and piglets following high-dose intravenous administration of an adeno-associated virus vector expressing human SMN. *Hum. Gene Ther.*, **29**, 285–298.
30. McBride, J.L., Boudreau, R.L., Harper, S.Q., Staber, P.D., Monteys, A.M., Martins, I., Gilmore, B.L., Burstein, H., Peluso, R.W., Polisky, B. *et al.* (2008) Artificial miRNAs mitigate shRNA-mediated toxicity in the brain: implications for the therapeutic development of RNAi. *Proc. Natl. Acad. Sci. U. S. A.*, **105**, 5868–5873.
31. Volak, A., LeRoy, S.G., Natasan, J.S., Park, D.J., Cheah, P.S., Maus, A., Fitzpatrick, Z., Hudry, E., Pinkham, K., Gandhi, S. *et al.* (2018) Virus vector-mediated genetic modification of brain tumor stromal cells after intravenous delivery. *J. Neuro-Oncol.*, **139**, 293–305.
32. Aschauer, D.F., Kreuz, S. and Rumpel, S. (2013) Analysis of transduction efficiency, tropism and axonal transport of AAV serotypes 1, 2, 5, 6, 8 and 9 in the mouse brain. *PLoS One*, **8**, e76310.
33. Budnik, V., Ruiz-Canada, C. and Wendler, F. (2016) Extracellular vesicles round off communication in the nervous system. *Nat. Rev. Neurosci.*, **17**, 160–172.
34. Zappulli, V., Friis, K.P., Fitzpatrick, Z., Maguire, C.A. and Breakefield, X.O. (2016) Extracellular vesicles and intercellular communication within the nervous system. *J. Clin. Invest.*, **126**, 1198–1207.
35. Zhang, A., Li, M., Wang, B., Klein, J.D., Price, S.R. and Wang, X.H. (2018) miRNA-23a/27a attenuates muscle atrophy and renal fibrosis through muscle-kidney crosstalk. *J. Cachexia. Sarcopenia Muscle*, **9**, 755–770.
36. Maes, M.E., Colombo, G., Schulz, R. and Siegert, S. (2019) Targeting microglia with lentivirus and AAV: recent advances and remaining challenges. *Neurosci. Lett.*, **707**, 134310.
37. Grace, P.M., Wang, X., Strand, K.A., Baratta, M.V., Zhang, Y., Galer, E.L., Yin, H., Maier, S.F. and Watkins, L.R. (2018) DREADDed microglia in pain: implications for spinal inflammatory signaling in male rats. *Exp. Neurol.*, **304**, 125–131.
38. Rosario, A.M., Cruz, P.E., Ceballos-Diaz, C., Strickland, M.R., Siemienski, Z., Pardo, M., Schob, K.L., Li, A., Aslanidi, G.V., Srivastava, A. *et al.* (2016) Microglia-specific targeting by novel capsid-modified AAV6 vectors. *Mol. Ther. Methods Clin. Dev.*, **3**, 16026.
39. Rossi, A., Dupaty, L., Aillot, L., Zhang, L., Gallien, C., Hallek, M., Odenthal, M., Adriouch, S., Salvetti, A. and Buning, H. (2019) Vector uncoating limits adeno-associated viral vector-mediated transduction of human dendritic cells and vector immunogenicity. *Sci. Rep.*, **9**, 3631.
40. Chakrabarty, P., Li, A., Ladd, T.B., Strickland, M.R., Koller, E.J., Burgess, J.D., Funk, C.C., Cruz, P.E., Allen, M., Yaroshenko, M. *et al.* (2018) TLR5 decoy receptor as a novel anti-amyloid therapeutic for Alzheimer's disease. *J. Exp. Med.*, **215**, 2247–2264.
41. Keren-Shaul, H., Spinrad, A., Weiner, A., Matcovitch-Natan, O., Dvir-Szternfeld, R., Ulland, T.K., David, E., Baruch, K., Lara-Astaiso, D., Toth, B. *et al.* (2017) A unique microglia type associated with restricting development of Alzheimer's disease. *Cell*, **169**, 1276–1290 e1217.
42. Kamphuis, W., Kooijman, L., Schetters, S., Orre, M. and Hol, E.M. (2016) Transcriptional profiling of CD11c-positive microglia accumulating around amyloid plaques in a mouse model for Alzheimer's disease. *Biochim. Biophys. Acta*, **1862**, 1847–1860.
43. Bamberger, M.E., Harris, M.E., McDonald, D.R., Husemann, J. and Landreth, G.E. (2003) A cell surface receptor complex for fibrillar beta-amyloid mediates microglial activation. *J. Neurosci.*, **23**, 2665–2674.
44. Koenigsknecht, J. and Landreth, G. (2004) Microglial phagocytosis of fibrillar beta-amyloid through a beta1 integrin-dependent mechanism. *J. Neurosci.*, **24**, 9838–9846.
45. Gitik, M., Liraz-Zaltsman, S., Oldenborg, P.A., Reichert, F. and Rotshenker, S. (2011) Myelin down-regulates myelin phagocytosis by microglia and macrophages through interactions between CD47 on myelin and SIRPalpha (signal regulatory protein-alpha) on phagocytes. *J. Neuroinflammation*, **8**, 24.
46. Fadok, V.A., Warner, M.L., Bratton, D.L. and Henson, P.M. (1998) CD36 is required for phagocytosis of apoptotic cells by human macrophages that use either a phosphatidylserine receptor or the vitronectin receptor (alpha v beta 3). *J. Immunol.*, **161**, 6250–6257.
47. Stuart, L.M., Bell, S.A., Stewart, C.R., Silver, J.M., Richard, J., Goss, J.L., Tseng, A.A., Zhang, A., El Khoury, J.B. and Moore, K.J. (2007) CD36 signals to the actin cytoskeleton and regulates microglial migration via a p130Cas complex. *J. Biol. Chem.*, **282**, 27392–27401.
48. Woo, M.S., Yang, J., Beltran, C. and Cho, S. (2016) Cell surface CD36 protein in monocyte/macrophage contributes to

phagocytosis during the resolution phase of ischemic stroke in mice. *J. Biol. Chem.*, **291**, 23654–23661.
49. Stewart, C.R., Stuart, L.M., Wilkinson, K., van Gils, J.M., Deng, J., Halle, A., Rayner, K.J., Boyer, L., Zhong, R., Frazier, W.A. *et al.* (2010) CD36 ligands promote sterile inflammation through assembly of a toll-like receptor 4 and 6 heterodimer. *Nat. Immunol.*, **11**, 155–161.
50. Wilkinson, K., Boyd, J.D., Glicksman, M., Moore, K.J. and El Khoury, J. (2011) A high content drug screen identifies ursolic acid as an inhibitor of amyloid beta protein interactions with its receptor CD36. *J. Biol. Chem.*, **286**, 34914–34922.
51. Tanzi, R.E. (2015) TREM2 and risk of Alzheimer's disease—friend or foe? *N. Engl. J. Med.*, **372**, 2564–2565.
52. Chan, G., White, C.C., Winn, P.A., Cimpean, M., Replogle, J.M., Glick, L.R., Cuerdon, N.E., Ryan, K.J., Johnson, K.A., Schneider, J.A. *et al.* (2015) CD33 modulates TREM2: convergence of Alzheimer loci. *Nat. Neurosci.*, **18**, 1556–1558.
53. Caso, J.R., Pradillo, J.M., Hurtado, O., Leza, J.C., Moro, M.A. and Lizasoain, I. (2008) Toll-like receptor 4 is involved in subacute stress-induced neuroinflammation and in the worsening of experimental stroke. *Stroke*, **39**, 1314–1320.
54. Park, J., Wetzel, I., Marriott, I., Dreau, D., D'Avanzo, C., Kim, D.Y., Tanzi, R.E. and Cho, H. (2018) A 3D human triculture system modeling neurodegeneration and neuroinflammation in Alzheimer's disease. *Nat. Neurosci.*, **21**, 941–951.
55. Hickman, S.E., Allison, E.K. and El Khoury, J. (2008) Microglial dysfunction and defective beta-amyloid clearance pathways in aging Alzheimer's disease mice. *J. Neurosci.*, **28**, 8354–8360.
56. Ishizuka, K., Kimura, T., Igata-Yi, R., Katsuragi, S., Takamatsu, J. and Miyakawa, T. (1997) Identification of monocyte chemoattractant protein-1 in senile plaques and reactive microglia of Alzheimer's disease. *Psychiatry Clin. Neurosci.*, **51**, 135–138.
57. El Khoury, J., Toft, M., Hickman, S.E., Means, T.K., Terada, K., Geula, C. and Luster, A.D. (2007) Ccr2 deficiency impairs microglial accumulation and accelerates progression of Alzheimer-like disease. *Nat. Med.*, **13**, 432–438.
58. El Khoury, J.B., Moore, K.J., Means, T.K., Leung, J., Terada, K., Toft, M., Freeman, M.W. and Luster, A.D. (2003) CD36 mediates the innate host response to beta-amyloid. *J. Exp. Med.*, **197**, 1657–1666.
59. Zhang, Y., Chen, K., Sloan, S.A., Bennett, M.L., Scholze, A.R., O'Keeffe, S., Phatnani, H.P., Guarnieri, P., Caneda, C., Ruderisch, N. *et al.* (2014) An RNA-sequencing transcriptome and splicing database of glia, neurons, and vascular cells of the cerebral cortex. *J. Neurosci.*, **34**, 11929–11947.
60. Roy, M., Richard, J.F., Dumas, A. and Vallieres, L. (2012) CXCL1 can be regulated by IL-6 and promotes granulocyte adhesion to brain capillaries during bacterial toxin exposure and encephalomyelitis. *J. Neuroinflammation*, **9**, 18.
61. Zhang, K., Tian, L., Liu, L., Feng, Y., Dong, Y.B., Li, B., Shang, D.S., Fang, W.G., Cao, Y.P. and Chen, Y.H. (2013) CXCL1 contributes to beta-amyloid-induced transendothelial migration of monocytes in Alzheimer's disease. *PLoS One*, **8**, e72744.
62. Maguire, C.A., Crommentuijn, M.H., Mu, D., Hudry, E., Serrano-Pozo, A., Hyman, B.T. and Tannous, B.A. (2013) Mouse gender influences brain transduction by intravascularly administered AAV9. *Mol. Ther.*, **21**, 1470–1471.